NTNU

Norwegian University of
Science and Technology

Assessment of Pipeline Integrity after Trawling Impact by Investigating Dent with Gouge

Agnes Karin Eliassen

Marine Technology
Submission date: June 2016
Supervisor: Sigmund Kyrre Ås, IMT
Co-supervisor: Mario Polanco-Loria, Statoil

Norwegian University of Science and Technology
Department of Marine Technology

NTNU Trondheim
Norges teknisk-naturvitenskapelige universitet
Institutt for marin teknikk

MASTER THESIS SPRING 2016

for

Stud. tech. Agnes Karin Eliassen

Assessment of pipeline integrity after trawling impact by investigating dent with gouge

Background

Interference between subsea pipelines and trawling equipment is a relatively common occurrence. While pipelines and protection measures are designed for impact, damage may occur that compromises the long-term integrity of the pipe. For more than 30 years a significant body of research has been collected in an effort to understand the failure mechanism of pipelines associated with defects such as dents, gouges, corrosion, bending wrinkles, and welding defects among others. With regard to outside damage, integrity assessment is based on the permanent dent depth as a percentage of the pipeline diameter. Scratches are not permitted, which is justified by the large fatigue life scatter in pipelines with both smooth dents and scratches/gouges. Pipelines under this category must therefore be repaired at great cost for the operator.

Scope of Work

This project will study the influence of dents and gouges on pipeline fatigue lives. The aim is to improve our understanding of the problem through numerical and experimental methods. Small-scale experiments will be conducted by applying cyclic internal pressure to damaged pipes, and finite element models will be applied to calibrate predictive models. Since the problem is quite involved, the scope of the project will have to be limited to what can be feasibly achieved within the time period. Possible topics for closer examination include both experimental and numerical topics:

- Measurement of dent and gouge geometry by 3D acquisition methods.
- Instrumentation by strain gauges and verification of FEA.
- Fatigue life prediction based on geometrical parameters and/or FEA stress solutions.

Thesis report

The thesis report should be organised in a rational manner to give a clear exposition of results, assessments, and conclusions. The text should be brief and to the point, with a clear language. Telegraphic language should be avoided.

The report shall be written in English and edited as a research report including literature survey, description of relevant mathematical models together with numerical simulation results, discussion, conclusions and proposal for further work. List of symbols and acronyms, references and (optional) appendices shall also be included. All figures, tables and equations shall be numerated.

The original contribution of the candidate and material taken from other sources shall be clearly defined. Work from other sources shall be properly referenced using an acknowledged referencing system.

Thesis supervisor**:**
Sigmund Kyrre Ås, NTNU
Mario Polanco-Loria, Statoil

Deadline: June 19th, 2016

Preface

The master thesis is a part of my five-year Master of Science education in Marine Technology at Norwegian University of Science and Technology (NTNU) in Trondheim.

Throughout the process there has been some problems regarding the software and the experimental work. Due to high activity in the lab the original scope had to change late in the semester to take into consideration the limited time available. In combination with some of the equipment had to be repaired the experimental work has taken longer than first presumed. However the thesis has been a interesting and I had a great learning outcome.

Trondheim, 2016-06-19

Agnes Karin Eliassen

Acknowledgements

I would like to thank my co-supervisor Sigmund Kyrre Ås at the Department of Marine Technology for guidance and help trough the semester. I would also show gratitude to my co-supervisor Mario Polanco-Loria at Statoil. He has contributed with up to date research on the area and Statoil has in addition supported the project financially.

I would like to give thanks to Emil Bratlie, Kristian Aamot and Kristian Minde at the lab at NTNU for assisting in building and running the experiments. Especially for staying later than expected in order to finish my work. I would also like to mention Alexander Hoel and Truls Bache for guidance using the ATOS 3D scanner and to Ann-Johanne Bjørgen at the library for help finding published literature.

At last I would like to thank my fellow students at C1.076 for motivation and support.

Abstract

Mechanical damage from trawling gear interference amongst others cause a significant amount of damage to pipelines. The present study has done a review of current standards and recommended practise for assessment methods for unconstrained plain dent with gouge. A test method was developed to investigate stress concentration factor and fatigue life of the combined damage with plain dent and gouge. Three different indenter shapes was created and indented four dents on two welded round precision tubes (E235+CR1) with a diameter/thickness ratio of 51. Three of them also contained a gouge. After denting, strain gauges was applied. The pipe samples was then pressurized to evaluate stress concentration factor (SCF).

A numerical model was created according to the experiment. The numerical model was consistent with the indention process, showing good results when comparing numerical and experimental results. The 3D acquisition tool Autodesk 123D Catch proved to be a good and efficient method to scan the pipe samples in order to create a three dimensional (3D) model. Numerical model predicted rerounding and dent depth at a satisfactory manner. Furthermore when comparing the strain gauges with numerical work with regards to SCF the model did not produce valid results. The strain gauges was located were the highest values for strain was expected to be, however it was shown that there might be locations with higher strains and the initially assumptions was mistaken. Therefore the numerical model needs improvement when investigating SCF and fatigue life.

Sammendrag

Skader fra tråleutstyr kan blant annet føre til en betydelig mengde med skader på rørledninger som ligger på havbunnen. Denne studien har gjort en gjennomgang av dagens standarder og anbefalt praksis for vurderingsmetoder for bulk med skrape. En forsøksmetode ble utviklet for å undersøke spenningskonsentrasjonfaktor og utmattingslevetiden for den kombinerte skade for bulk med skrape. Tre forskjellige indenter geometrier ble lagd og fire bulker ble fordelt på to stålrør (E235+CR1) med diameter/tykkelseforhold på 51. Tre av dem inneholdt også en skrape. Etter bulking, ble det satt på strekklapper. Rørene ble deretter trykket opp for å vurdere spenningskonsentrasjonfaktor.

Den numeriske modellen var i overensstemmelse med bulkeprosessen, og viser gode resultater når man sammenligner numeriske og eksperimentelle resultater. 3D-verktøyet Autodesk 123D Catch viste seg å være en god og effektiv metode for å skanne røret for å skape en 3D-modell. Numerisk modell gjenskapte "rerounding" og bulk dybde på en tilfredsstillende måte. Videre når man sammenligner strekklappene med numerisk modell med hensyn til spenningskonsentrasjonfaktor, produserte den ikke gode nok resultater. Strekklappene var plassert der de høyeste verdiene for tøyning var forventet, men det ble vist at dette ikke var i samsvar der det faktisk var størst tøyning. Det ble vist at den numeriske modellen må forbedres når undersøker SCF og utmatting.

Contents

List of Figures

List of Tables

Abbreviations

2D	two dimensional
3D	three dimensional
API	American Petroleum Institute
ASME	American Society of Mechanical Engineers
CONCAWE	European Oil Company Organisation for Environment Health and Safety
CSA	Canadian Standards Association
DNV	Det Norske Veritas
EGIG	European Gas pipeline Incident data Group
EPRG	European Pipeline Research Group
FE	finite element
FEM	finite element method
GT	Georgia Institute of Technology
JIP	joint industry project
LVDT	linear variable differential transformer
NTNU	Norwegian University of Science and Technology
PDAM	Pipeline Defect Assessment Manual
PRCI	Pipeline Research Council International
SCF	stress concentration factor

Nomenclature

$2c$	length of gouge	$[m]$
A	fracture area of a $\frac{2}{3}$ Charpy specimen	$[mm^2]$
a_1	constants	$[-]$
a_2	constants	$[-]$
ϕ	angle between strain gauges	$[rad]$
B	factor	$[-]$
l	constraint factor	$[-]$
α	correction factor	$[-]$
C_v	Charpy energy	$[J]$
D	pipe external diameter	$[m]$
d	dent depth measured at zero pressure	$[m]$
d_p	dent depth measured at pressure	$[m]$
E	elastic modulus	$[Pa]$
ε	strain	$[-]$
σ	stress	$[Pa]$
E_t	tangent modulus	$[Pa]$
H	maximum depth of gouge	$[m]$
H'	plastic tangent modulus	$[Pa]$
K_t	theoretical stress concentration factor	$[-]$
K_1	correction factor	$[-]$
K_2	correction factor	$[-]$

K_f	fatigue stress concentration factor	$[-]$
K_d	factor	$[m]$
L	dent length	$[m]$
N	cycles to failure	$[-]$
ν	poisson ratio	$[-]$
P	pressure	$[bar]$
Q	parameter	$[-]$
q	notch sensitivity factor	$[-]$
R	stress ratio	$[-]$
r_m	average radius	$[m]$
τ	shear stress	$[Pa]$
σ_A	equivalent stress	$[Pa]$
σ_a	alternating stress	$[Pa]$
σ_C	failure stress	$[Pa]$
σ_{eff}	effective stress	$[Pa]$
σ_f	flow stress	$[Pa]$
σ_m	mean stress	$[Pa]$
σ_{max}	maximum stress	$[Pa]$
σ_{min}	minimum stress	$[Pa]$
$\sigma_{N,C}$	circumferential fracture stress	$[Pa]$
$\sigma_{N,L}$	effective net stress	$[Pa]$
σ_{nom}	nominell stress	$[Pa]$
σ_u	ultimate tensile strength	$[Pa]$
σ_y	yield strength	$[Pa]$
t	pipe wall thickness	$[m]$
ε_e	elastic strain	$[-]$
ε_p	plastic strain	$[-]$

σ_v	von Mises stress	$[Pa]$
Y_1	correction factor	$[-]$
Y_2	correction factor	$[-]$

Chapter 1

Introduction

1.1 Background

Interference between trawling equipment and subsea pipeline is a common occurrence in the oil and gas industry. See Figure 1.1 for illustration. Therefore the pipelines are designed for impact, however an allowable impact load may inflict damage that compromise the long-term integrity.

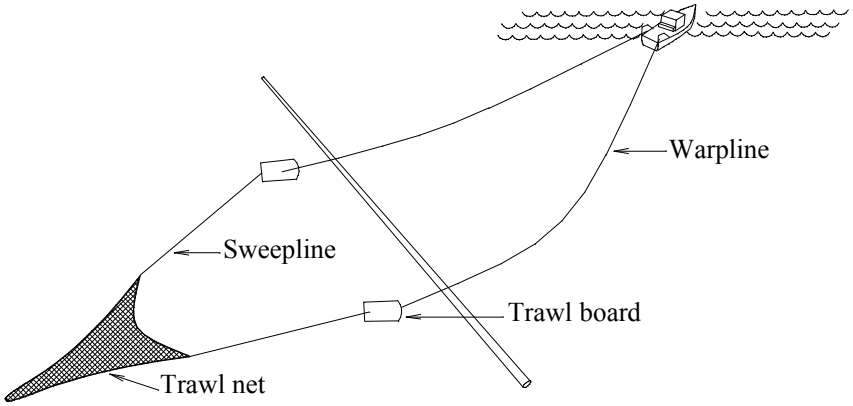

Figure 1.1: Trawling gear inteference with pipeline (DNV, 2014)

For more than 40 years a tremendous amount of research has been done in order to understand the failure mechanism of pipelines. These are associated with dents, gouges, corrosion, kinks etc. Today's standard allow to some extent a dent in the pipeline, however

if the dent includes a gouge/scratch it is not permitted. Such damage is complicated as it introduces both high stress concentration factor (SCF) and possible local corrosion, due to the possibility of penetration of the protection coating. The cost of repair is high due to all the offshore and subsea operations required. Table 1.1 summarizes the distribution of incidents. The distribution of incidents in gas (between 2004-2013) is from the annual report published by European Gas pipeline Incident data Group (EGIG) (2016) and from incidents with oil (from 1971-2012) pipelines from European Oil Company Organisation for Environment Health and Safety (CONCAWE) report by den Haan and Davis (2014). For the latter mechanical damage and 3rd party interference is merged to external interference.

Table 1.1: Distribution of incidents

Pipeline:	External interference	Corrosion	Construction defects/ material failures	Ground movement	Other
Gas	35 %	24 %	16 %	13 %	12 %
Oil (Hot)	13 %	81 %	N/A	N/A	6 %
Oil (Cold)	71 %	19 %	N/A	N/A	10 %

It shows a great deal of the damage to pipeline is mechanical damage and interference, and shows the importance of understanding the significance of the combination of dent with gouge.

1.2 Definitions of terms

The Pipeline Defect Assessment Manual (PDAM) (Cosham and Hopkins, 2006, p. 161-201) defines the following terms:

dent a depression which produces a gross disturbance in the curvature of the pipe wall,

caused by contact with a foreign body, resulting in plastic deformation of the pipe wall.

plain dent a smooth dent that contains no wall thickness reductions (such as a gouge or a crack) and does not change the curvature of an adjacent girth weld or seam weld.

unconstrained dent a dent that is free to rebound elastically (spring back) when the indenter is removed, and is free to reround as the internal pressure varies.

constrained dent a dent that is not free to rebound or reround, because the indenter is not removed. A rock dent is an example of a constrained dent.

gouge a surface damage to a pipeline caused by contact with a foreign object that has displaced or removed material from the pipe wall, resulting in a metal loss defect.

Figure 1.2 illustrates the dent dimensions: dent depth measured at zero pressure (d), pipe external diameter (D), dent length (L), pipe wall thickness (t), maximum depth of gouge (H) and length of gouge ($2c$).

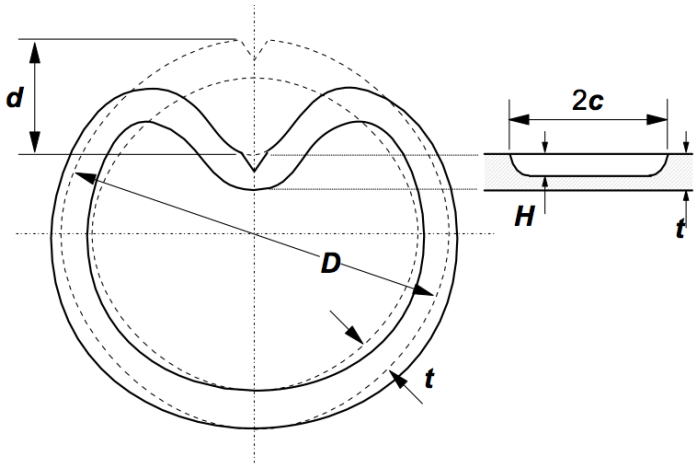

Figure 1.2: Dent dimensions (Cosham and Hopkins, 2006)

1.3 Objective

The objective is to investigate how the geometry of the object will impact the SCF when introducing a dent with a gouge. Of particular interest is whether it is possible to create geometrically similar dents with and without scratches. This will allow experimental comparison of fatigue lives for such dents.

1.4 Scope and limitations

The scope of the thesis is:

- Do a review of current standards, recommended practise and current research on assessment methods for unconstrained plain dents with a gouge.
- Develop small-scale test methods for evaluating SCF and fatigue life of pipelines with gouges.
- Through experiments damage steel pipelines with different indenter geometries, introducing a dent with a gouge. Apply internal pressure to create a realistic scenario for transporting pipelines. Find SCF for the different cases.
- Use finite element (FE) to create a numerical model of the denting process and pressurization

The fatigue life testing was not done due to time constraints by the lab personnel, hence a limitation for the scope.

1.5 Published literature

Over the past 40 years there has been several studies to clarify the impact a dent has on a pipeline. Few mentions the combination dent and a gouge. The presence of a gouge

is classified as a severe form for damage according to Cosham and Hopkins (2006). The movement due to spring back and rerounding will cause large amount of stress and strain at the base of the gouge and lead to initiation and growth of cracks. The gouging process will have the consequence that the base of the gouge will be cold worked. This area may contain cracking and the work hardened layer will have reduced ductility. In general a dent with gouge is difficult to assess. Alexander (1999) gives the primary reasons for the complexity in predicting burst pressure, listed below. A suggestion for further investigations is to vary one parameter and keep the other constant.

- Material properties (especially ductility and toughness)
- Sharpness and depth of gouge
- Pressure at indention and during rerounding
- Dent profile and depth, as well as resulting plastic deformation of the pipe
- Local work-hardening and variations in through-wall properties

The traditional acceptance criteria is 6 % dent depth of D, however a dent with mechanical damage should not be accepted based solely on this according to Rosenfeld et al. (2002). Even dents or scrape that seems too superficial to matter could be dangerous. Alexander (1999) presented previous research, see Table 1.2 showing that the presence of a gouge significantly reduces fatigue life when applied cyclic internal pressure. However when only the gouge is present it is non-threatening, which contradict Rosenfeld et al. assertion.

Table 1.2: Fatigue life for gouges, plain dents and dents with gouges (Alexander, 1999)

Dent depth	Gouge depth	Fatigue Life
% of D	% of t	cycles to failure (N)
0	20	> 145 500
4	0	< 6 930
4 (in weld)	0	< 789
4	20	< 119

Of interest in the article written by Rosenfeld et al. (2002) is the assessment of gouge and dent. A typical damage is depicted in Figure 1.3, a damage from excavating equipment (Rosenfeld et al., 2002).

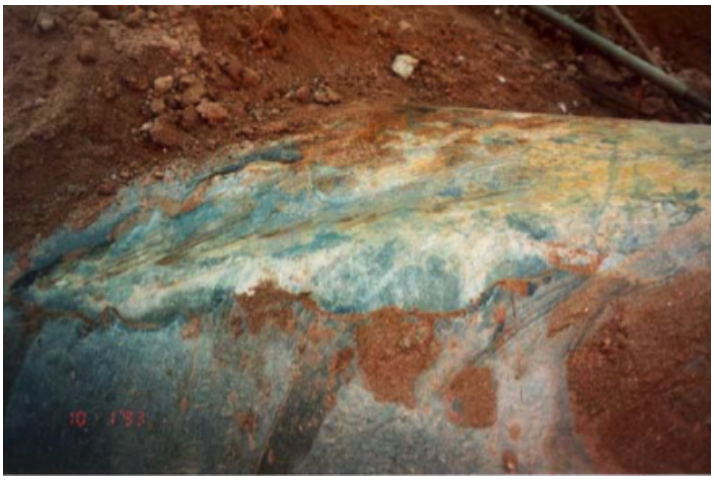

Figure 1.3: Typical dent and gouge (Rosenfeld et al., 2002)

Even though there has been over four hundred full scale test when the article by Rosenfeld et al. (2002) was published, there is no model that accurately predicts the failure pressure or fatigue life of dent with gouge. It is only conservative approaches and with good margins of safety. The difficulty to predict the damage is due to that the severity of the dent is dependent on how and when the dent or/and gouge is introduced.

Allouti et al. (2014) investigated A37 steel pipelines with combined dent and gouge. Both numerical and experimental methods was used and compared, to conclude that it do not reduce the burst pressure. A example of how the stress distribution is ahead of the gouge tip is shown in Figure 1.4 based on finite element analysis. Here both dent with a gouge and a gouge alone is represented, the α is representing the slope. Allouti et al. (2014) states that this supports the assumption that the dent with gouge can be treated as a gouge alone using the volumetric method. The difference in slopes that can be seen is bending moments from the dent wall moving with pressure.

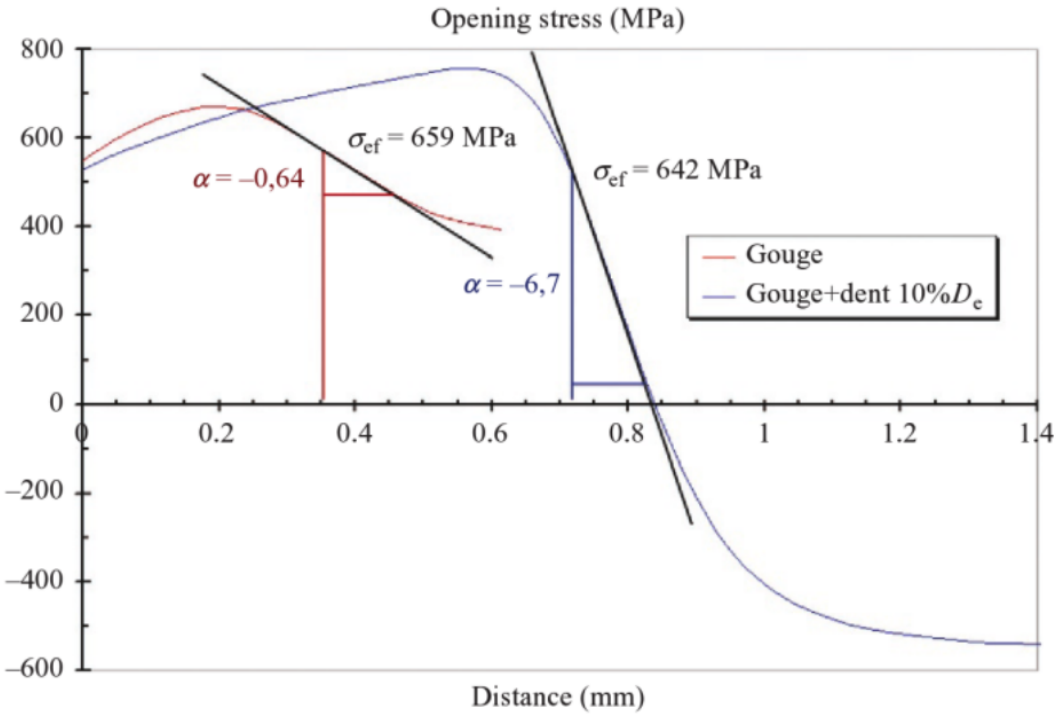

Figure 1.4: Stress distrubution ahead of defect tip (Allouti et al., 2014)

In the Figure D_e is denoted D in the present study. The effective stress (σ_{eff}) is the average value of the stress distribution inside the fracture process zone. Allouti et al. suggest a combined criterion for assessing pipelines with a dent and gouge defect, which should be based on volumetric method and stress triaxiality.

Chapter 2

Mechanical behaviour of materials

The basic concepts, definitions and theory relevant for the present study is described in this chapter.

2.1 Elastisity and plasticity

The typical strain stress curve for a elasto-plastic material is found in Figure 2.1. The curve displays the material behaviour in three regions of behaviour from start of loading to fracture. It defines tangent modulus (E_t), elastic modulus (E), elastic strain (ε_e), plastic strain (ε_p) with regards to a stress (σ)-strain (ε) plot. Furthermore the figure denotes de_p and de_e as the change of ε_p and ε_e respectively.

From start to point 1, the material exhibits linear elastic behaviour. Here the relationship between strain and stress is linear, and the gradient is E. It can be described by Hooke's law (Dowling, 1998) given in Equation 2.1 with σ and ε.

$$\sigma = E\varepsilon \tag{2.1}$$

In this area the material will not suffer any permanent deformation as it is in the elastic area. After passing point 2 the strain is a combination of ε_e and ε_p, given in Equation 2.2.

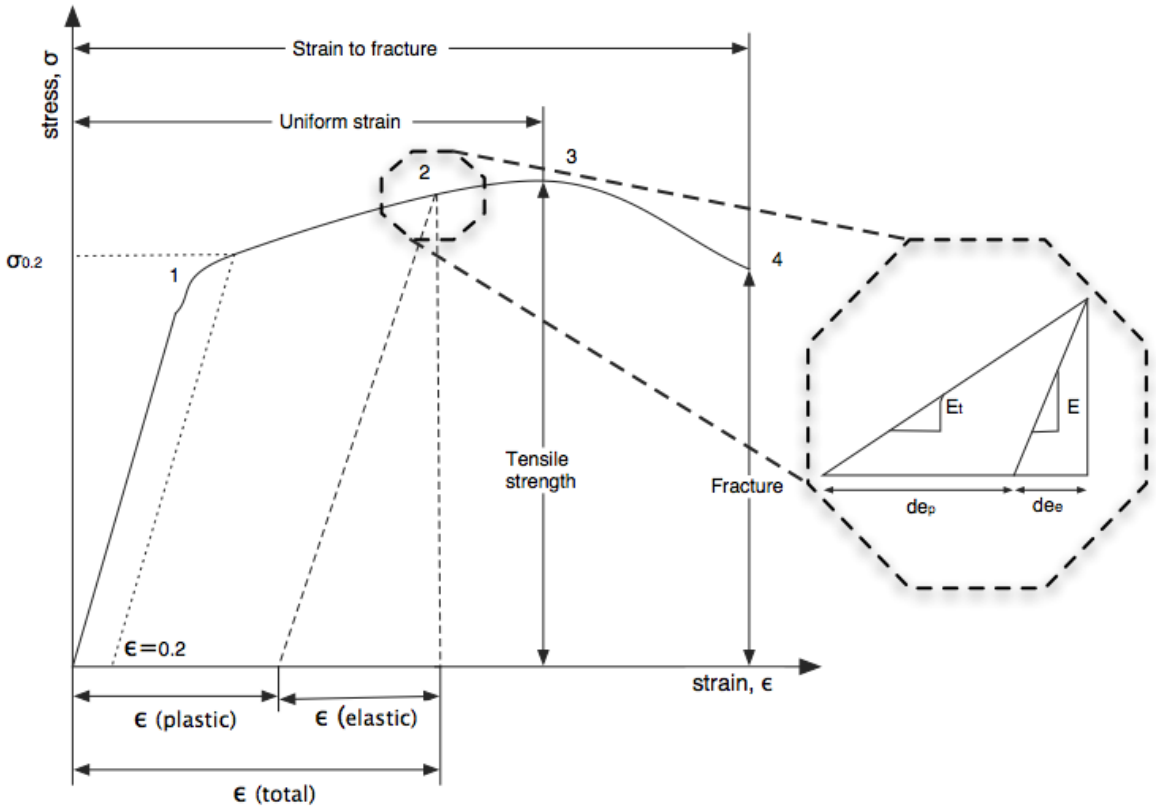

Figure 2.1: The typical behaviour of elasto-plastic material (Eliassen, 2007)

$$\varepsilon = \varepsilon_p + \varepsilon_e \tag{2.2}$$

Now the curve has a rising curve indicating the hardening of the material. If the material had been a perfect plastic material, this line would have been horizontal. If the component is unloaded somewhere between point 1 and 2, it would follow a parallel line to the elastic loading curve. When the component have removed the load, only the plastic part remains. Hence the stress increment $d\sigma$ can be written as Equation 2.3.

$$d\sigma = E d\varepsilon_e = H' d\varepsilon_p = E_t d\varepsilon \tag{2.3}$$

where plastic tangent modulus (H') is defined by Equation 2.4.

$$H' = \frac{1}{\frac{1}{E_t} - \frac{1}{E}} \tag{2.4}$$

It is also in this area the yield strength (σ_y) is found. It is hard to obtain the exact value, therefore it common to define it by 0.2 % of ε as in the figure. The ultimate tensile strength (σ_u) is defined at point 3, and is the highest stress the material can be loaded.

2.1.1 Hooke's law in three dimensional (3D)

Hooke's law can be extended for three dimensions by considering the six stress components depicted in Figure 2.2. It includes the stresses in three directions: σ_X, σ_Y (not to be confused with σ_y) and σ_Z, and shear stress (τ) in three direction τ_{xy}, τ_{yz} and τ_{zx}.

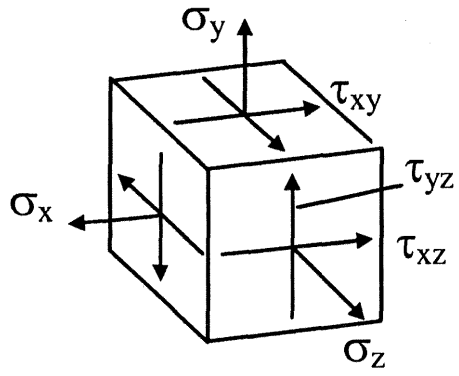

Figure 2.2: Stress components Berge (2006a)

In order to obtain the stresses for three dimensions, it is necessary to include poisson ratio (ν) as expressed in Equation 2.5.

$$\nu = -\frac{\varepsilon_y}{\varepsilon_x} \tag{2.5}$$

Then Hooke's law in three dimensions is given in Equation 2.6. It should be noted that E

and ν are constant to be used as useful approximations (Dowling, 1998).

$$\begin{bmatrix} \sigma_X \\ \sigma_Y \\ \sigma_Z \\ \tau_{yz} \\ \tau_{xz} \\ \tau_{xy} \end{bmatrix} = \frac{E}{(1+\nu)(1-2\nu)} \begin{bmatrix} 1-\nu & \nu & \nu & 0 & 0 & 0 \\ \nu & 1-\nu & \nu & 0 & 0 & 0 \\ \nu & \nu & 1-\nu & 0 & 0 & 0 \\ 0 & 0 & 0 & \frac{1-2\nu}{2} & 0 & 0 \\ 0 & 0 & 0 & 0 & \frac{1-2\nu}{2} & 0 \\ 0 & 0 & 0 & 0 & 0 & \frac{1-2\nu}{2} \end{bmatrix} \begin{bmatrix} \varepsilon_x \\ \varepsilon_y \\ \varepsilon_z \\ 2\varepsilon_{yz} \\ 2\varepsilon_{xz} \\ 2\varepsilon_{xy} \end{bmatrix} \tag{2.6}$$

2.2 Stress concentration

The fatigue life of a material is strongly affected by holes, corners, notches etc. These are more commonly called stress concentrations. A SCF allows the fatigue analysis to be executed by using nominell stress (σ_{nom}). Nominell stress is the stress measured at the original cross section area. The theoretical stress concentration factor (K_t) is given in Equation 2.7 with maximum stress (σ_{max}).

$$K_t = \frac{\sigma_{max}}{\sigma_{nom}} \tag{2.7}$$

Not all materials are fully sensitive to notches and therefore a reduced value of K_t can be utilized. The fatigue stress concentration factor (K_f) is defined by Equation 2.8.

$$K_f = \frac{\text{maximum stress in notches specimen}}{\text{stress in notch-free specimen}} \tag{2.8}$$

A relation between K_t and K_f can be found by introducing the notch sensitivity factor (q) as done in Equation 2.9.

$$K_f = 1 + q(K_t - 1) \tag{2.9}$$

The variable q varies from material properties, and can be found in Shigley et al. (2004) amongst others. There is however some uncertainty in the correct value of q, and the safest option is to assume that $K_t = K_f$.

There is no standard method for determining the SCF in the published literature known to the author. According to Alexander and Jorritsma (2010) the best solution for finding SCF is first to use an analytically-derived method to estimate SCF and then verify experimentally. The drawback is that the methods are time consuming and often expensive.

Ong et al. (1992) investigated the effects of strains of a local dent on a pressurized pipe. The behaviour of short dents differ from long dents, as the location of the peak stress is at different location. For a long dent, it is centred in the root of the dent, whereas for the plain dent it is located at the dent shoulder. The plain dent has in general a lower peak stress. According to (Rinehart and Keating, 2002), when the dent depth increases, the peak stress moves from the root of the dent, along the axial axis away from the center. The stress concentration in a dent is shown in Figure 2.3.

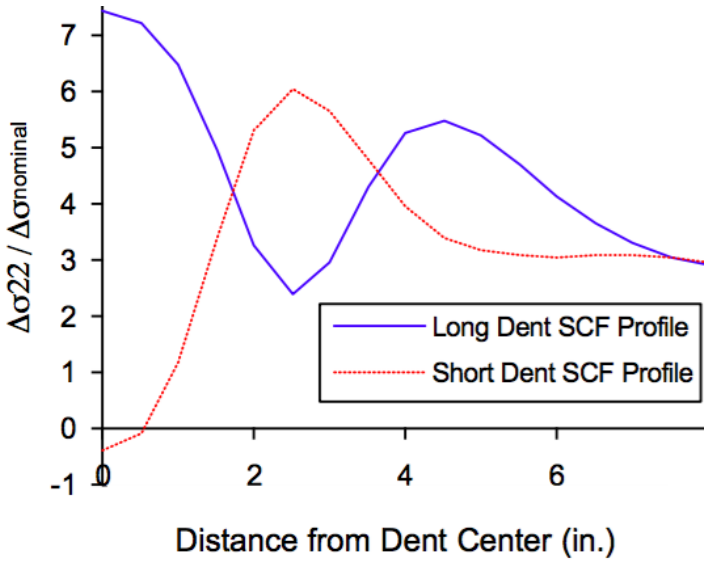

Figure 2.3: Outer surface stress concentration profiles (Rinehart and Keating, 2002)

The long dent is 7.5 % $\frac{d}{D}$ and the short dent is 17.5 % $\frac{d}{D}$. The dent shoulder is around 5.08 to 7.62 centimetre away from the dent center for the short dent, and the dent center ends between 7.62 and 10.16 centimetre for the long dent. Note that the figure the distance is in inches, 1 inch is equal to 2.54 centimetres. σ_{22} defines the stress in radial direction.

2.3 Spring back and rerounding

If a pipeline is experiencing an impact from an object, the denting involves both a plastic and elastic response in the material. This means that when the object is removed, the elastic component of the deformation is recovered and the dent depth is reduced. This phenomena is termed spring back. Rerounding is when the dent depth is changed by internal pressure. As the internal pressure increases, the dent depth decreases. The magnitude of the stress cycles and material properties decides if the rerounding is plastic or elastic according to Rosenfeld (1998). The stress and strain distribution changes when the dent experiences rerounding. Both the phenomena spring back and rerounding is illus-

trated in Figure 2.4, note that d is termed with H_0 in the figure, following then H_p is equal to dent depth measured at pressure (d_p), H_r is dent depth at rerounding.

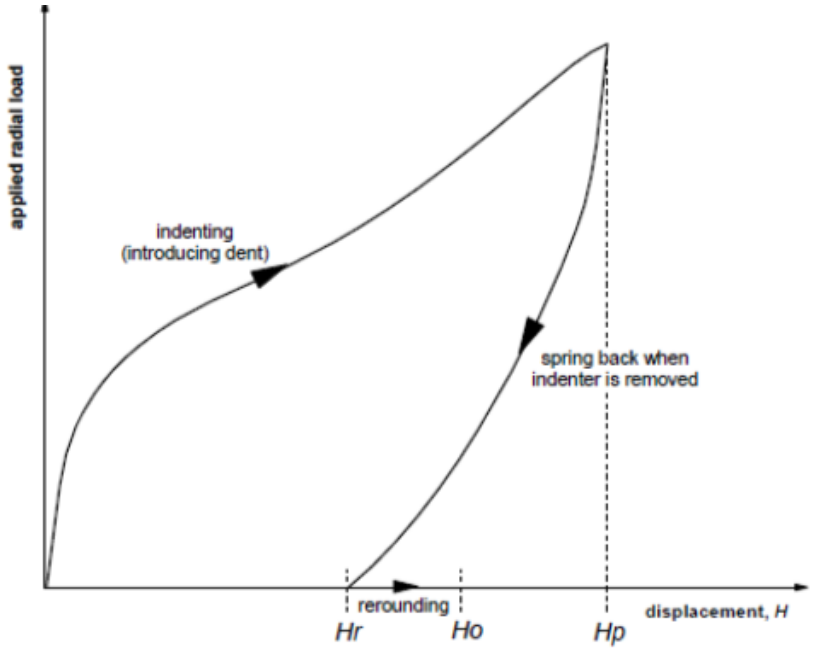

Figure 2.4: Rerounding and spring back from Cosham and Hopkins (2006)

The current rules and assessment method is based on a non-pressurized dent depth, and several correction factor for the rerounding effect has been developed. Race (2008) points out that most of them do not take into account all aspects that will contribute, and there is a lot of scatter in the existing test data. The most commonly used criteria is derived by European Pipeline Research Group (EPRG), and is shown in Equation 2.10 (Roovers et al., 2000) with d_p.

$$d = 1.43 d_p \tag{2.10}$$

Equation 2.10 only take dent depth into account, which is viewed to be a conservative and not realistic approach. Therefore the new criteria was developed by results from finite element method and confirmed with experiments. Le Bastard (2006) presented a new

criteria which take into account more aspects such as the pressure (P). The criteria is presented in Equation 2.11 with σ_y.

$$d = \pi d_p \frac{1}{\pi - 2\alpha arctan(\frac{L}{d_p}) arctan(0.1 \frac{D}{t} \frac{P}{\sigma_Y})} \tag{2.11}$$

where

$$\alpha = a_1 (\frac{d_p}{L})^{a_2} \tag{2.12}$$

The correction factor (α), given in Equation 2.12 contains two constants, a_1 and a_2, which are not given in the article by Le Bastard (2006). The correction factor is there to act as a safety factor. The criteria shows good results for lowering the threshold, and gives an improved assessment which is less conservative. However, as Race (2008) points out, the constants are not published so it can not be compared with other published data.

2.4 von Mises yield criterion

When a component is subjected to complex loadings so that in a given point the stresses may occur in several directions. If these stresses are severe, the combination of stresses may cause the material to yield or fracture. Hence a yield criteria is necessary in order to predict yielding. The von Mises yield criterion for plane stress is used to evaluate the combination of stresses. The von Mises stress (σ_v) is presented in Equation 2.13.

$$\sigma_v = \sqrt{\sigma_x^2 - \sigma_x \sigma_y + \sigma_y^2 + 3\sigma_{xy}^2} \tag{2.13}$$

For a thin walled pipeline the von Mises stress is given in Equation 2.14. Here is average radius (r_m) used.

$$\sigma_v = \frac{\sqrt{3}}{2}\frac{Pr_m}{t} \tag{2.14}$$

2.5 Notch-impact tests

The resistance of a material ability to resist sudden fracture where a sharp stress raiser or flaw is present is provided trough notch-impact tests. The most common type is Charpy V-notch test (Dowling, 1998). The ability to resist sudden fracture is measured by the energy required to break the sample is denoted Charpy energy (C_v). This is done by a pendulum raised to release a impact on the test specimen. C_v is used as a part of assessment for gouges for some criterias. The fracture area of a $\frac{2}{3}$ Charpy specimen (A) is commonly 53.55 mm^2.

2.6 Fatigue

The definition of the stresses in a fatigue load history is presented in Figure 2.5. It defines alternating stress (σ_a), σ_{max}, minimum stress (σ_{min}) and mean stress (σ_m).

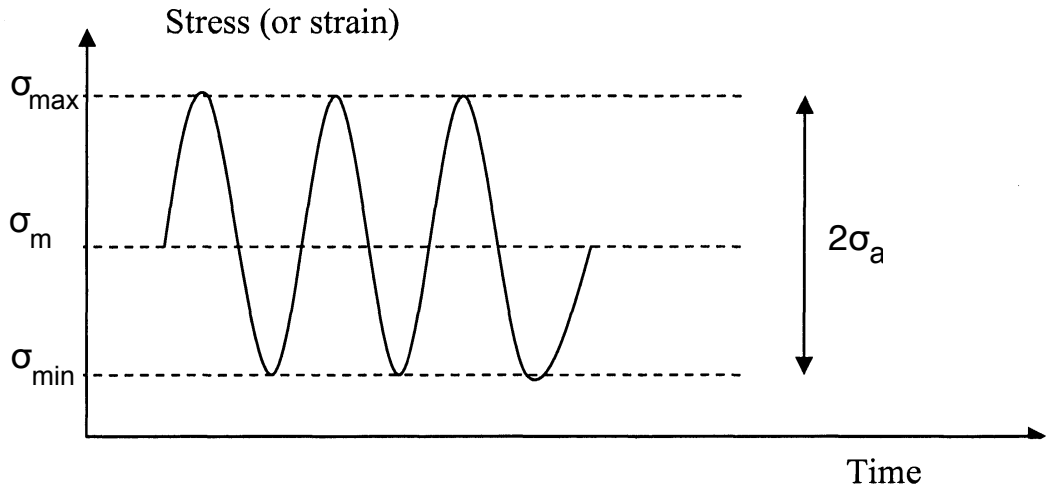

Figure 2.5: Stresses in a fatigue load cycle

The stress ratio (R) is defined by Equation 2.15. Then equivalent stress (σ_A) is defined when $R = 0$, which means that the cyclic load is repeated and in one direction, when the stress cycles goes from 0 to σ_{max}.

$$R = \frac{\sigma_{min}}{\sigma_{max}} \tag{2.15}$$

For predicting the fatigue life there is two methods that are commonly used for dented pipelines. Either by using S-N curves or fracture mechanics, applying empirical or semi-empirical models. The S-N curve is the most common to use, and will be explained briefly.

A cyclic stress (S) against logarithmic scale of N curve, or S-N curve as it is more commonly named, predicts cycles to failure. S-N curves are derived from material testing, where the material is applied cyclic stress to failure. Figure 2.6 shows an example of a S-N curve. The stress concentration in a dent can be accounted for by utilizing a SCF to the cyclic stress range. Then the N, can be found from the S-N curve, in other words the fatigue life of the dented pipeline.

A constraint for using the S-N curve is that the resulting plot is only valid for the test conditions. The S-N curve should not be used to predict real life behaviour if it deviates from the test conditions according to Stone (2012).

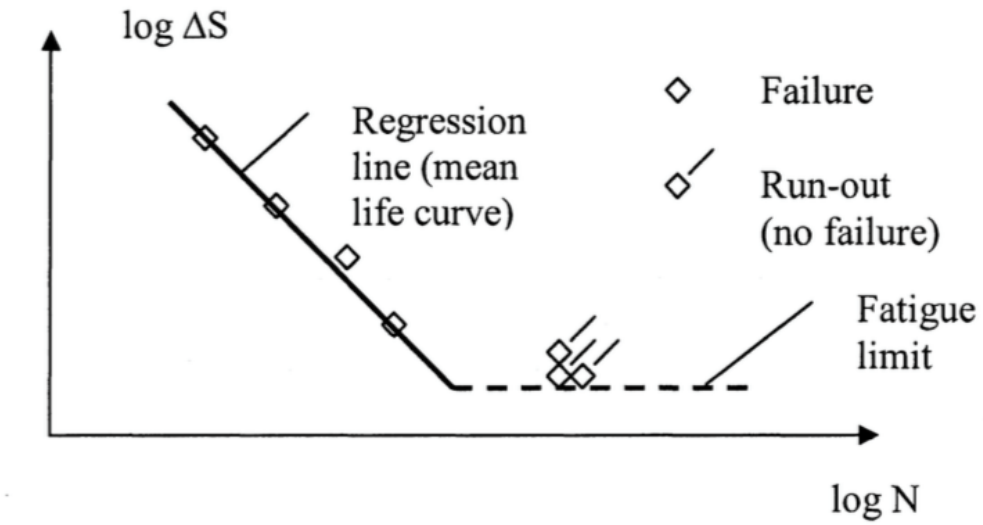

Figure 2.6: S-N curve with individual test data (Berge, 2006b)

Chapter 3

Assessment methodologies and governing standards

Several empirical relationship to assess plain dent with a gouge has been proposed by British Gas, European Pipeline Research Group (EPRG) via PDAM and Battelle via Pipeline Research Council International (PRCI). These methods will be presented in this chapter together with the most common standards.

3.1 Batelle Institute

The Batelle Institute (Allouti et al., 2014) for PRCI presented in a report from 1981 a empirical relationship utulizing the Charpy energy (C_v). It is based on failure stress (σ_C) and a parameter (Q) for the C_v. This was based on 30 full scale burst test (Cosham and Hopkins, 2001). Equation 3.1 is based on burst test results with flow stress (σ_f).

$$\frac{\sigma_C}{\sigma_f} = \frac{(Q-300)^{0.6}}{90} \tag{3.1}$$

The σ_f is defined by Equation 3.2.

$$\sigma_f = \sigma_Y + 69Mpa \tag{3.2}$$

The Q is defined by Equation 3.3. The dent geometry is defined in Figure 1.2.

$$Q = \frac{C_v}{\left(\frac{d}{D}\right)2c\left(\frac{H}{t}\right)} \tag{3.3}$$

This method has a limitation to $Q > 300$ ft lbf in^{-1}, or $Q > 16\,014$ J/m in SI units.

3.2 PDAM

In 1998 a joint industry project (JIP), was initiated to create PDAM (Cosham and Hopkins, 2006). The purpose was to create a manual collecting and evaluating all the published literature with regard to assessment of dents in pipelines. The result is a 479 pages long document which works as a guideline for the industry. The main purpose is to provide a tool for how to assess the severity of the dent, and how to assess the impact on fatigue life. In general, it provides results for onshore and offshore transmission pipelines which are design according to an international standard (Cosham and Hopkins, 2006, p. 3) and most of the industry use it as a guidebook. The method proposed to assess plain dent and dent with gouges according to PDAM is presented.

3.2.1 Plain dent

The EPRG, has published two methods in order to predict the fatigue life, the 1995 version and the 2000 version. The background of the 1995 version is unknown (Cunha et al., 2014) and the 2000 version is based on 131 fatigue test into DIN 2413 Part 1 SN curve (Roovers et al., 2000). Both methods will be presented here.

The 1995 version is the one recommended by PDAM for unconstrained plain dents, since it is more accurate than the 2000 version when the results are compared to test data (Cosham and Hopkins, 2006, p. 169). The fatigue life is calculated by the following equations taken

from the PDAM.

$$N = 1000\left[\frac{(\sigma_U - 50)}{2\sigma_A K_t}\right]^{4.292} \tag{3.4}$$

with σ_u and σ_A found in Equation 3.5

$$2\sigma_A = \sigma_U\left[B(4+B^2)^{0.5} - B^2\right] \tag{3.5}$$

The factor (B) is found by Equation 3.6, where R is given by Equation 2.15.

$$B = \frac{\frac{\sigma_a}{\sigma_U}}{\left[1-\left(\frac{\sigma_{max}-\sigma_a}{\sigma_U}\right)\right]^{0.5}} = \frac{\frac{\sigma_a}{\sigma_U}}{\left[1-\frac{\sigma_a}{\sigma_U}\left(\frac{1+R}{1-R}\right)\right]^{0.5}} \tag{3.6}$$

$$K_t = 2.871\sqrt{K_d} \tag{3.7}$$

With the factor (K_d) is given in Equation 3.8.

$$K_d = d\frac{t}{D} \tag{3.8}$$

The 2000 version is a empirical model fitting, and the fatigue life is calculated with the following equations taken from Roovers et al. (2000, p. 415):

$$N = 5622\left[\frac{\sigma_U}{2\sigma_A K}\right]^{5.26} \tag{3.9}$$

where

$$K = 1 + 2\sqrt{d^{1.5}\frac{t}{D}} \tag{3.10}$$

$$\sigma_A = \frac{\sigma_a}{1-\left(\frac{\sigma_{max}-\sigma_a}{\sigma_U}\right)} \tag{3.11}$$

3.2.2 Dent with gouge

The assessment procedure according to Cosham and Hopkins (2006) is given in Figure 3.1. The figure shows that assessment of dent with gouge is a fairly complex procedure, and often a specialist advice is necessary. As shown to in the figure, PDAM recommends that if there is a dent with gouge, it can be estimated as done in section 3.2.1 (corresponding to section 25.10 in PDAM) by reducing the fatigue life by a factor of one hundred (Cosham and Hopkins, 2006, p. 217). The recommendation from PDAM is also to account for the possibility of cracking at the base by increasing the measured depth by 0.5 mm. A exception is when a inspection technique is used at the base of the gouge to detect and measure the cracking. Further, it has some limitations:

- Maximum depth of the gouge can maximum be 20 % of the wall thickness
- Maximum depth of the gouge can maximum be 4 % of the pipe diameter at zero pressure
- The $\frac{2}{3}$ thickness specimen size upper shelf C_v is at least 47 joules

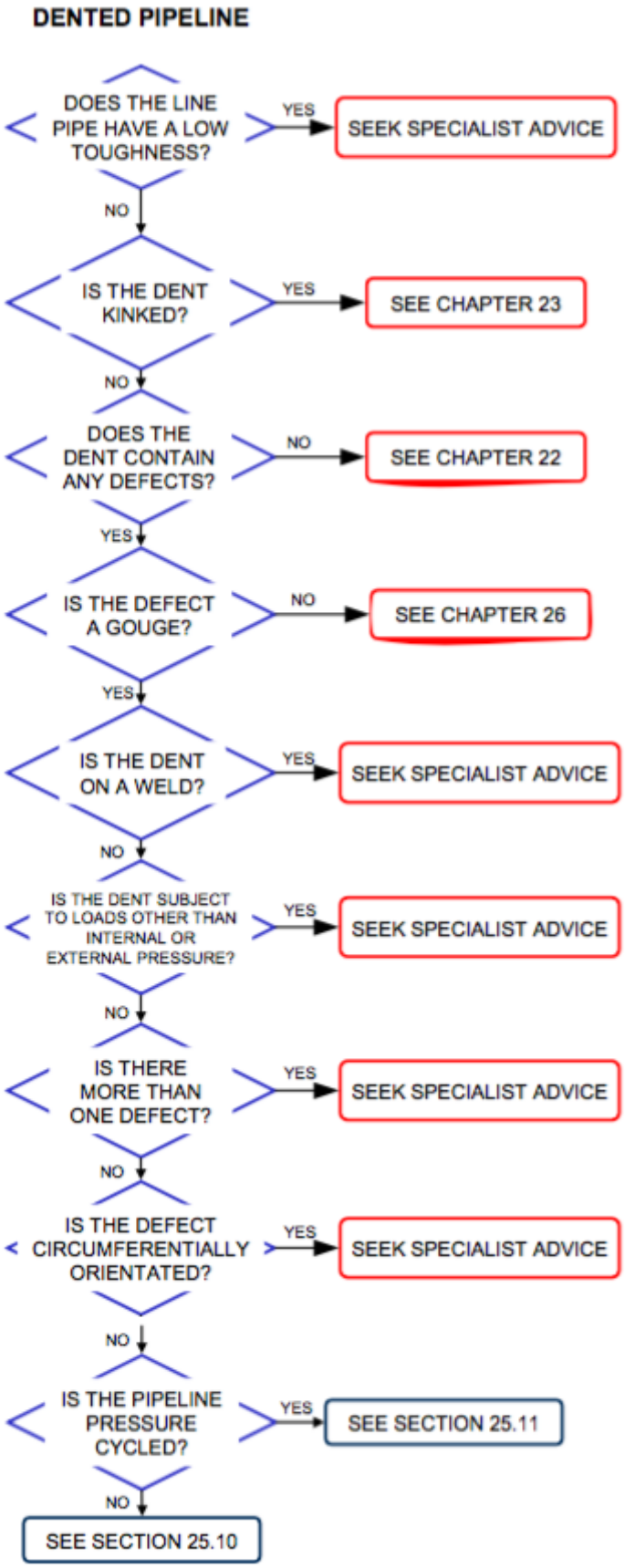

Figure 3.1: The assessment of a smooth dent containing a gouge (Cosham and Hopkins, 2006)

Figure 3.2 shows how this methodology is compared to published full scale testing of rings and vessels containing dents containing a gouge. Therefore PDAM regards this as the best method (Cosham and Hopkins, 2006, p. 217).

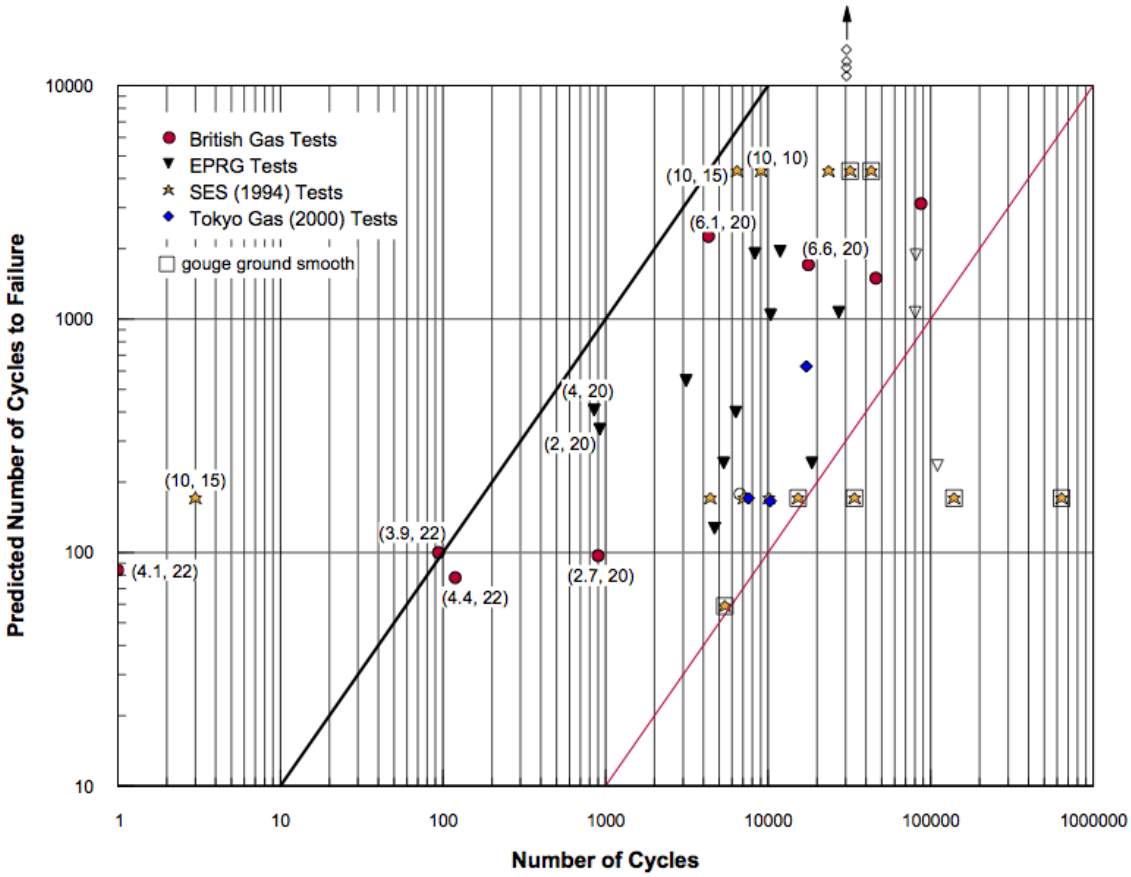

Figure 3.2: Predictions of the fatigue life of a smooth dent containing a 'gouge' made using the recommended method (dent depth after spring back for SES tests)(Cosham and Hopkins, 2006)

3.3 British Gas

British Gas Allouti et al. (2014) suggest a very complex formula, which determines the circumferential fracture stress ($\sigma_{N,C}$) of a pipe with a dent and a gouge. It utilises on a collapse modified strip yield model. The formula is expressed in Equation 3.12.

$$\frac{\sigma_{N,C}}{\sigma_{N,L}} = \frac{2}{\pi} cos^{-1}\left[exp\left\{ 113 \frac{1.5\pi E}{\sigma_f^2 AH}\left[Y_1\left(1 - 1.8\frac{d}{D}\right) + Y_2\left(10.2\frac{Rd}{tD}\right)\right]^2 exp\left[\frac{ln(0.738C_v) - K_1}{K_2}\right]\right\}\right] \tag{3.12}$$

The correction factors Y_1, Y_2, K_1 and K_2 is presented in Equation 3.13 together with the expression for effective net stress ($\sigma_{N,L}$).

$$\begin{aligned} \sigma_{N,L} &= 1.15\sigma_Y(1 - \frac{H}{t}) \\ Y_1 &= 1.12 - 0.23\frac{H}{t} + 7.32\frac{H^2}{t} - 13.1\frac{H^3}{t} + 14\frac{H^4}{t} \\ Y_2 &= 1.12 - 1.39\frac{H}{t} + 7.32\frac{H^2}{t} - 13.1\frac{H^3}{t} + 14\frac{H^4}{t} \\ K_1 &= 1.9 \\ K_2 &= 0.57 \end{aligned} \tag{3.13}$$

One should note the constraint factor (l) is equal to 1.15 in the Equation for $\sigma_{N,L}$. It is a more complex alternative method compared to the one presented in PDAM, and is the best method in term of fit with the published full scale test according to Cosham and Hopkins (2006).

3.4 Standards

Besides PDAM the different standards has defined acceptance criteria for plain dents, and dent with gouges. The list of the different standards are shown below.

- American Petroleum Institute (API) 1156 by Alexander and Kiefner (1997)
- American Society of Mechanical Engineers (ASME) B31.4 Code - Liquid Transportation Systems for Hydrocarbons, Liquid Petroleum Gas, Anhydrous Ammonia, and Alcohols (ASME, 1992, p. 59)

- ASME B31.8 Code - Gas Transmission and Distribution Piping Systems (ASME, 2014, p. 79)
- EPRG by Roovers et al. (2000, p. 412)
- Det Norske Veritas (DNV) in RP-F111: Interference between trawl gear and pipelines (DNV, 2014)
- Canadian Standards Association (CSA) (Race, 2008)

The criteria from different standards are summarized in Table 3.1. None of them allows dent with gouge. According to Alexander (1999) it is well known across the industry that these regulations are to be over conservative, by evaluating the research done on the matter.

Table 3.1: Summary of dent acceptance standards

	Plain Dents		**Dents with**
	Constrained	**Unconstrained**	**cracks or gouges**
API 1156 (1997)	Upto 6 % of D, > 2 % requires fatigue assessment		Not allowed
ASME B31.8 (2014)	Upto 6 % of D or not exceed 6 % strain		Not allowed
ASME B31.4 (1992)	Upto 6 % of D or strain level upto 6 % for OD > 4”		Not allowed
	Up to 6 mm in pipes with D < 4”		
DNV (2010)	3.5 % of D with low impact frequency		Not allowed
EPRG (2000)	≤ 7 % of D at a hoop stress of 72 % SMYS		Not allowed
CSA - Z662 (1999)	Upto 6 mm for ≤ 101.6 mm D or		Not allowed
	< 6 % of D for > 101.6 mm		

Chapter 4

Experimental method

In order to investigate the different dent geometries and the strain caused by internal pressure when a gouge is introduced, experimental methods are applied. A test procedure is developed to evaluate SCF and fatigue life. The pipe samples are damaged with the different shaped indenter's to create different dent geometries, then pressurized with internal pressure. The pipe dimensions, material properties and indenter's are introduced. The testing was done at laboratory at Norwegian University of Science and Technology (NTNU).

4.1 Material

Two pipe samples was welded round precision tube (E235+CR1) with the dimensions t = 2 mm and D = 102 mm. The ends on the pipeline was welded with end caps on each end. The material properties of pipe samples was obtained through uniaxial tension test. Two samples was tested in the axial direction, and three samples in the radial direction. The radial test specimen was manually flatten before testing. Figure 4.1 shows the testing apparatus (Figure 4.1a) and one of the test specimen (Figure 4.1b) with one extensometer.

(a) The testing apparatus

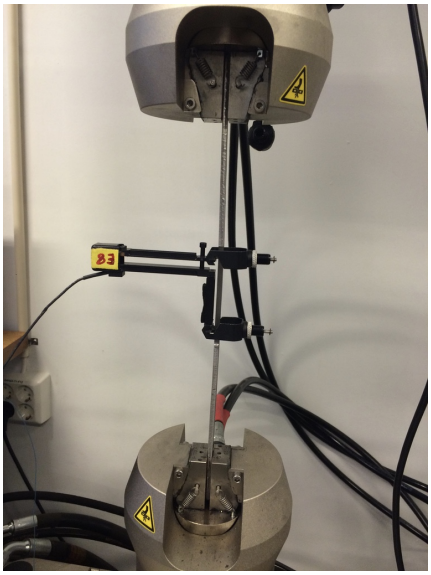

(b) Material testing specimen

Figure 4.1: Material testing

The values for E, σ_y and σ_u of failures are listed in table 4.1 for both longitudinal and axial direction. The σ_y is taken as 0.2 % of ε_p. The values are mean of all the tests done in each direction.

Table 4.1: Average material properties

Direction	E [GPa]	σ_y [MPa]	σ_u [MPa]
Axial	230.18	347.47	399.49
Radial	215.00	343.81	396.00

Figure 4.2 and 4.3 are the ε-σ plots for the different material and directions developed from the material testing.

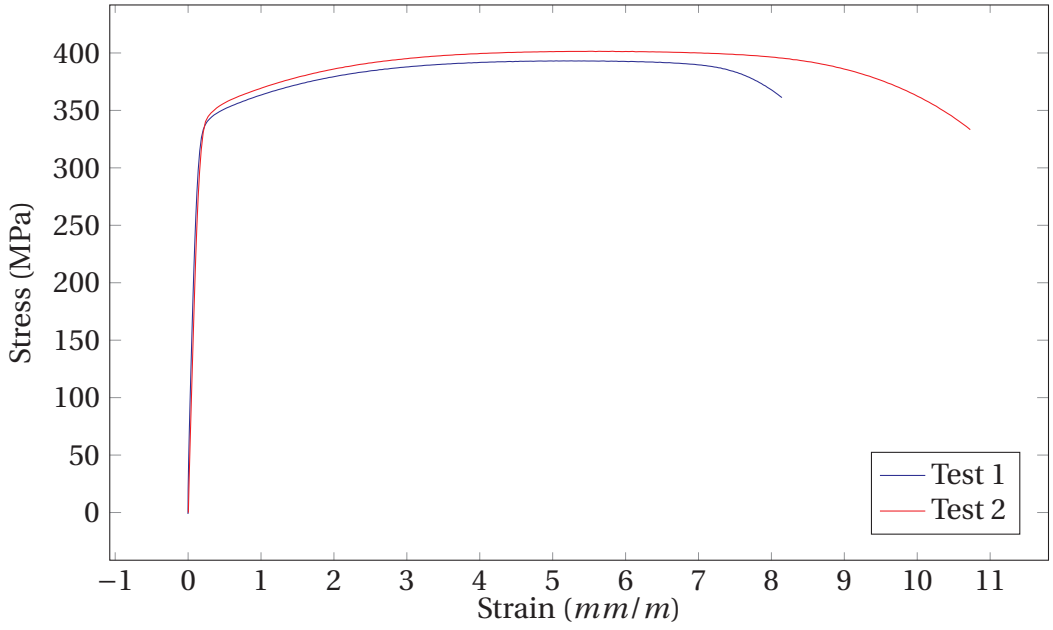

Figure 4.2: ε-σ in axial direction

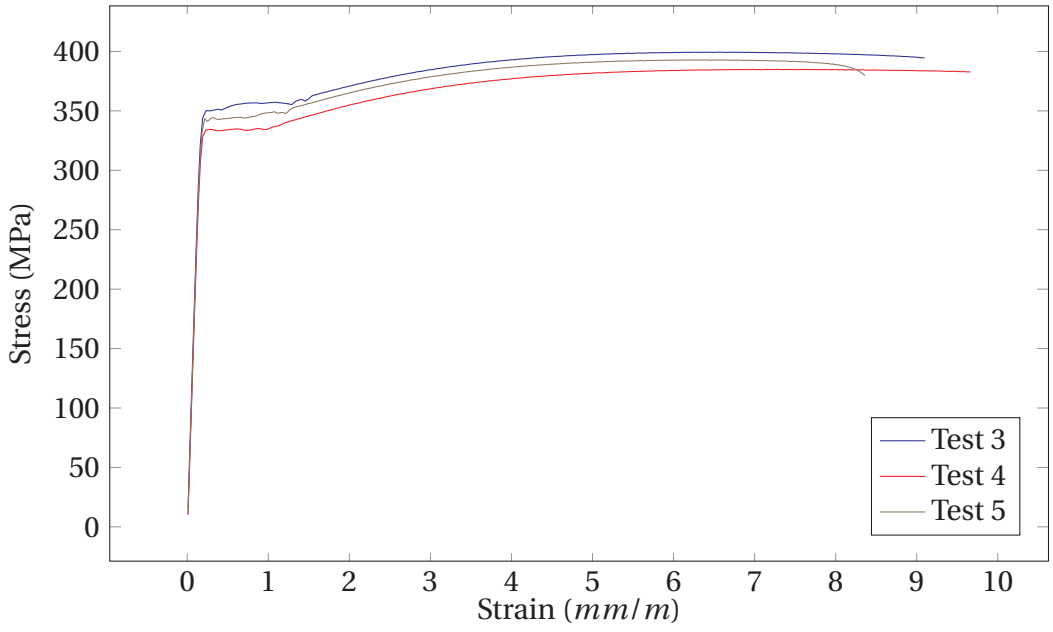

Figure 4.3: ε-σ in radial direction

4.2 Indenter process

The various dent geometries are presented in Figure 4.4.

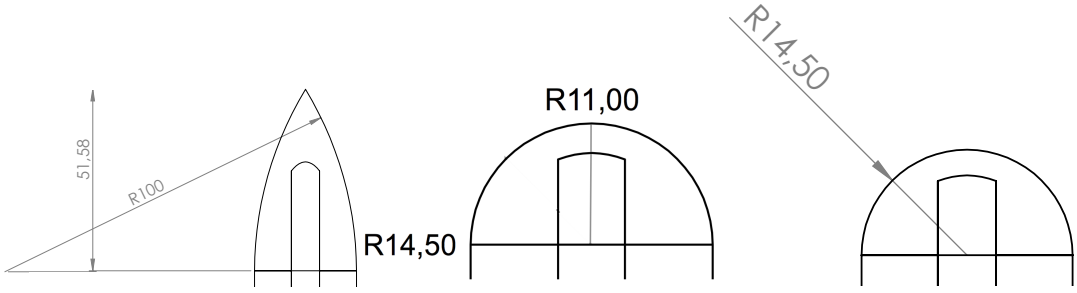

(a) Indenter 1 (b) Indenter 2 (c) Indenter 3

Figure 4.4: The different dent geometries used in experimental work

All the indenter are designed to have a diameter of 29 millimetres at the base. The set-up for the denting process is illustrated in Figure 4.5. On the top there is two holes with different distance from center, to obtain the dent depth 4 % and 8 % of D. It should be specified that the indenter's are pushed trough the side of the pipeline. In the present study the dent depth was approximated to 8 % of D.

Figure 4.5: Indenting process

The gouges was created by damaging the indenter's, as depicted in Figure 4.6.

(a) Indenter 1 with damage (b) Indenter 2 with damage (c) Indenter 3 with damage

Figure 4.6: The damage on indenter's to create gouges

The two pipe samples was dented as illustrated in Figure 4.7a and 4.7b. To make the ex-

periment more time efficient the second run was done with three dents. An assumption is made that when the dents are evenly distributed from each other and the pipe end, they will not interfere with each other. The length of the pipe samples was 1 000 mm and 1 500 mm for run 1 and 2 respectively. The blue half circles are illustrating the locating of the dents.

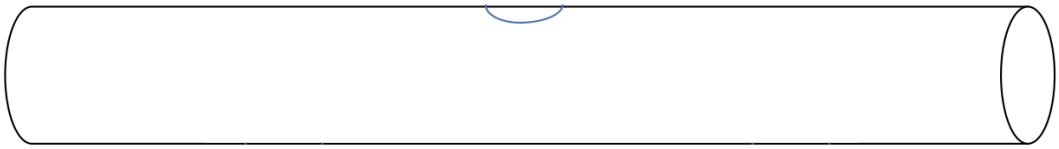

(a) Pipe sample for first run

(b) Pipe sample for second run

Figure 4.7: Pipe samples

The dent geometries before internal pressure is applied is shown in Figure 4.8. Note that Figure 4.8a is before gouge is applied. Dent I from Figure 4.8a is on pipe sample in Figure 4.7a, used for the first run. Dent II-IV in Figure 4.8b-4.8d is applied to pipe sample in Figure 4.7b used in the second run.

(a) Dent I from indenter 2

(b) Dent II from indenter 1

(c) Dent III from indenter 3

(d) Dent IV from indenter 3

Figure 4.8: The dents before internal pressure was applied

4.3 Test set-up

The test set-up consisted of a servo-hydraulic machine that actuated a hydraulic cylinder, which gave the test sample a harmonic oscillating pressure. The purpose is to apply internal pressure and obtain the strains and stresses in the dented area. The set-up is displayed in Figure 4.9, with the pipe sample laying outside the red pipe used as protection in case of a pressure blow-out. A linear variable differential transformer (LVDT) was used to measure the change in dent depth.

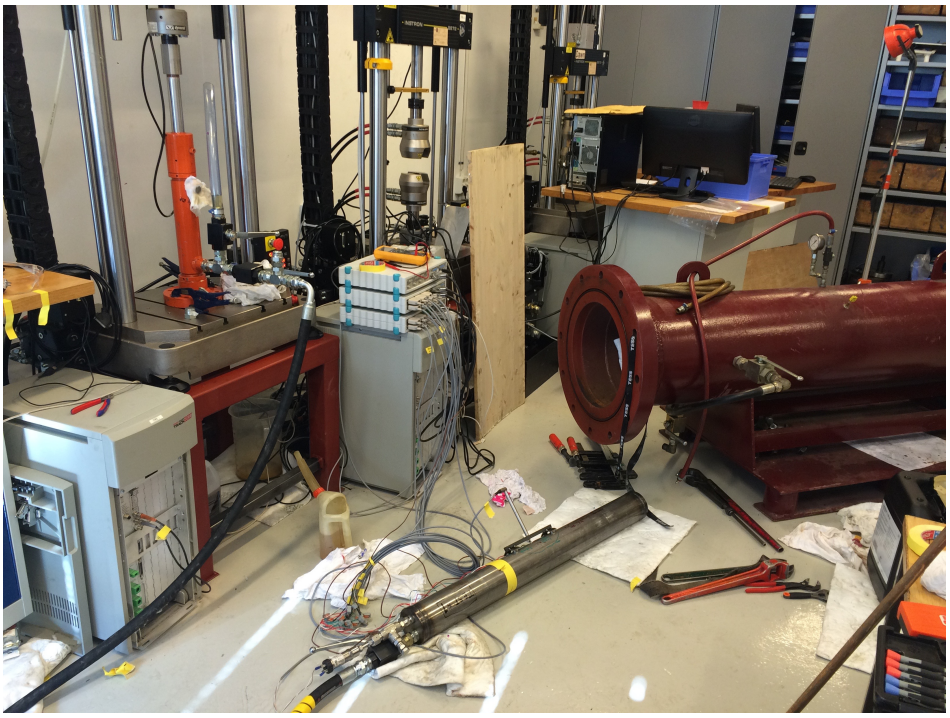

Figure 4.9: Test set-up

4.4 Test procedure

Three runs of the test was conducted, using the pipe samples depicted in Figure 4.7. The third run was done similar to the second run, just with new strain gauges, just with one

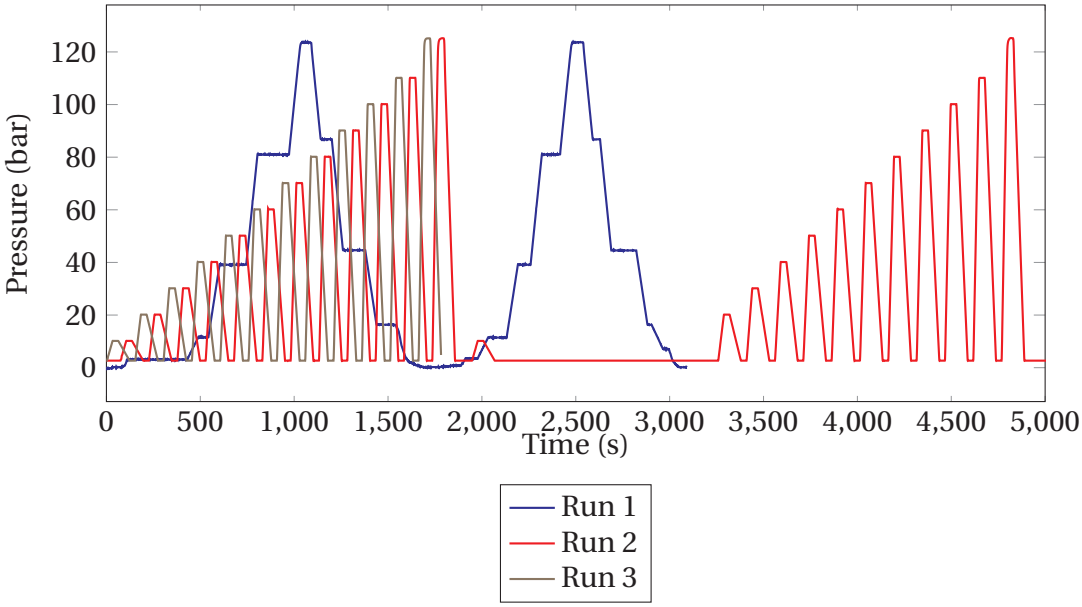

Figure 4.10: Pressure over time

pressure series. The pipe samples was pressurized in two series for the first two runs, as shown in Figure 4.10, where it is slowly pressured up to 125 bar. The second run the pressure was taken down to 0 bar between the pressure levels.

4.5 Strain gauges

To measure the strains in the pipe sample strain gauges was utilized. Therefore to measure the full state of strain, and to obtain von Mises stresses, it is necessary to measure ε_X, ε_Y and γ_{XY}. The most common method to obtain the strains in all directions is to apply a rosette gauge and measure at three different points with 45 degrees apart as shown in Figure 4.11. Here the strains from the rosette gauge is denoted ε_A, ε_B and ε_C, and angle between strain gauges (ϕ).

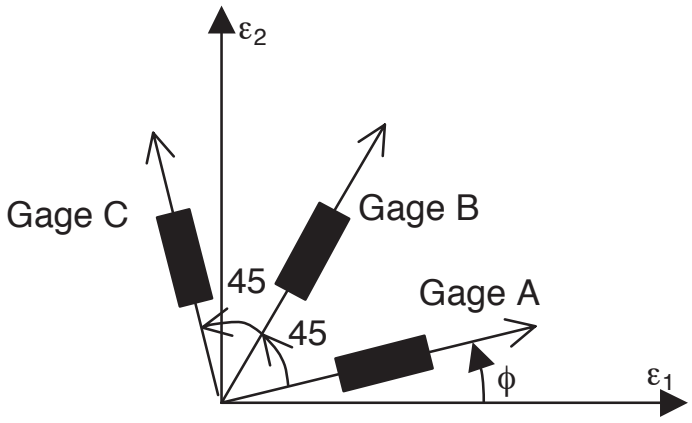

Figure 4.11: Rosette gauge orientation (Georgia Institute of Technology, 2000)

The two dimensional strain transformation equation are given in Equation 4.1 and taken from Georgia Institute of Technology (2000).

$$\begin{aligned} \varepsilon_A &= \varepsilon_X cos^2\phi + \varepsilon_Y sin^2\phi + \gamma_{XY} sin\phi cos\phi \\ \varepsilon_B &= 2(\varepsilon_Y - \varepsilon_X) sin\phi cos\phi + \gamma_{XY}(cos^2\phi - sin^2\phi) \\ \varepsilon_C &= \varepsilon_X sin^2\phi + \varepsilon_Y cos^2\phi - \gamma_{XY} sin\phi cos\phi \end{aligned} \tag{4.1}$$

The simplest way to calculate the strains is to orient the gauge such that gauge A is located along the x-axis, then following gauge C is located at the y-axis. Then Equation 4.1 can be simplified and rearranged to archive Equation 4.2.

$$\begin{aligned} \varepsilon_X &= \varepsilon_A \\ \varepsilon_Y &= \varepsilon_C \\ \varepsilon_{XY} &= 2\varepsilon_B - \varepsilon_A - \varepsilon_C \end{aligned} \tag{4.2}$$

The strain gauges was applied on the test sample where the highest strain values was expected to appear in early numerical analysis. Strain gauge 1 represent the highest strain, following strain gauge 2 is the second highest area for strain change. Table 4.2 shows the

coordinates of the strain gauges all except one. Dent I had a third gauge located and the dent shoulder, where the pipe wall starts to slope towards the dent. Look at Figure 4.12a. The coordinate system is in xz-plane, where z is in axial direction and x is in radial direction. The indention of the dent is in negative x-direction.

Table 4.2: Coordinates of strain gauges

	Gouge 1		Gouge 2	
	x (mm)	z (mm)	x (mm)	y (mm)
Dent I	-6.3 mm	11.9 mm	22.4 mm	2.5 mm
Dent II	0.0 mm	10.6 mm	-2.2 mm	1.6 mm
Dent III and IV	8.4 mm	11.9 mm	2.1 mm	14.9 mm

Figure 4.12 shows where the strain gauges was applied for the different dents. It should be noted that that Figure 4.12c and 4.12d is taken after internal pressure is applied. Also the strain gauges are placed on the same location for the two dents created by indenter 3 (dent III and IV). Since the strain gauges was applied after the denting process, it does not measure the residual stresses in the pipe sample prior to the pressurizing. Hence there is a simplification to the problem when looking at the strains later.

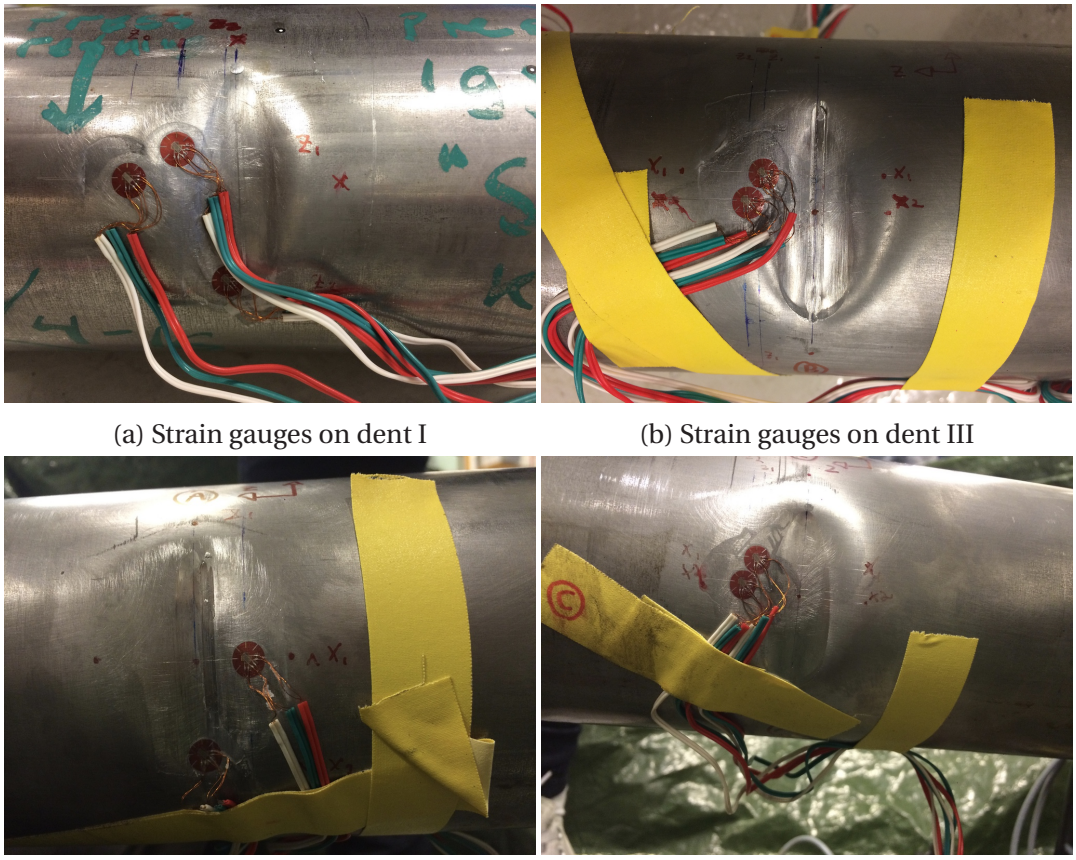

(a) Strain gauges on dent I

(b) Strain gauges on dent III

(c) Strain gauges on dent II

(d) Strain gauges on dent IV

Figure 4.12: Strain gauges on the pipe samples

4.6 3D acquisition methods

To ensure that the numerical model is correctly depicting the dented region as a result of the three different indenter geometries, it is verified with the data from a 3D surface scanner. Two methods was used to obtain 3D surface model. The ATOS industrial optical 3D scanner was used at one of NTNU's laboratory, and the app Autodesk 123D Catch was used for acquisition of a 3D model. Both methods utilizes close range photogrammetry. The main difference is the quality of the equipment. The main difference is that ATOS industrial optical 3D scanner uses two cameras whereas Autodesk 123D Catch uses the

one camera on the phone. A example of a scanned 3D model from ATOS is shown in Figure 4.13.

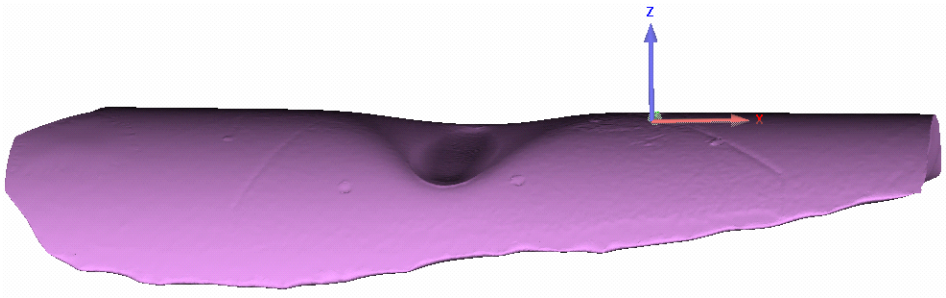

Figure 4.13: 3D model of dented pipeline

4.7 Results

A example of strains from the experimental work is presented in Figure 4.14.

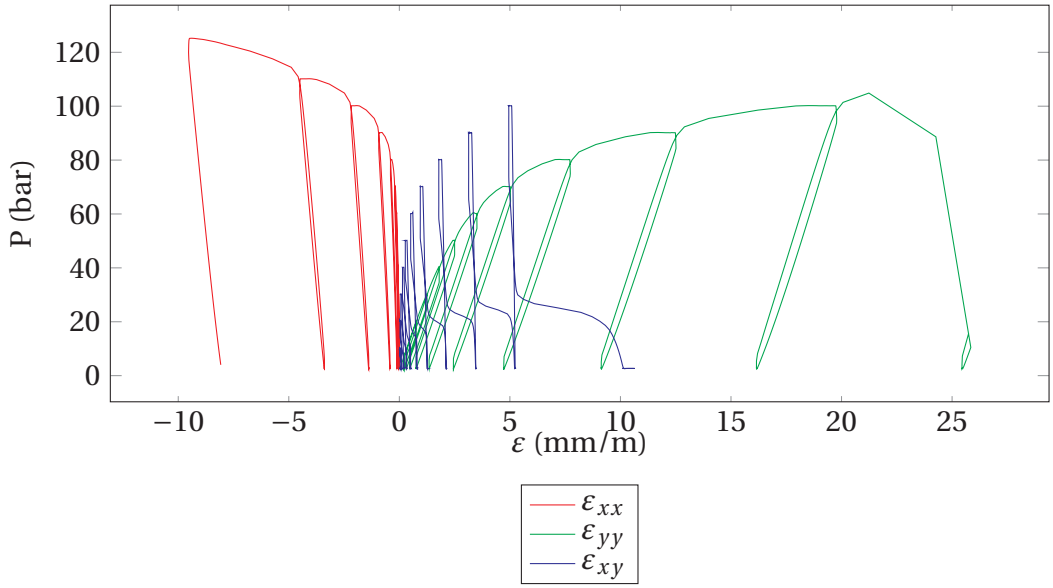

Figure 4.14: ε in dent III versus internal pressure - Gauge 2

Here the coordinate system is defined with x in axial direction and y in radial direction.

Some of the strain gauges in the experiments reached saturation, and therefore the graphs has varying amount of data. The rest of the are found in Appendix E. Only the strains from the first cycle is presented in the in Figure E.1 - E.9, as five out of six reached saturation in one direction and therefore the gauge was not of interest for the rest of the cycle. The raw data from the three experimental runs are presented in Appendix A, B and C.

Chapter 5

Numerical model

A numerical model was developed using ABAQUS/standard (Hibbitt et al., 2001). It solves the problem implicit. It consist of an 3D solid element model to represent the pipe system, and a shell model to represent the block for the indention process and the indenter's.

5.1 Finite element analysis

In order to verify the experimental results and compare how the gouge affect the SCF, finite element method (FEM) is utilised. A short introduction will cover the basis. Most of the engineering problems are complicated to solved by classical methods with an arbitrary shape. Since most cases can be modelled by differential equations, hence they can be solved by a numerical approach. The FEM is a numerical approach which uses the differential equations to approximate the solution.

The basic idea is to divide the shape into FE, connected by nodes. The collection of these are referred to as FE mesh. Then a solution can be approximated. If the differential equations are assumed to be valid over a certain region, they can be divided into FE. This means that if the problem is non-linear over the entire region, it can be assumed to be linear over a FE (Fish and Belytschko, 2007).

5.2 Model geometry

The numerical analysis consist of a global model in three parts: the pipe surface, the clamp to simulate the block and the indenter as shown in Figure 5.1. The clamp and indenter is meshed with rigid shell elements (R3D4), the pipe is modelled with solid elements (C3D8RH). The indenter and pipeline are designed according to the dimension used in the fatigue testing. The clamp is to simulate the block the pipe was in during the indention process, as seen in Figure 4.5. The indenter had three different geometries, presented in Section 4.1. Only half the pipeline was modelled in order to reduce the computational cost of the numerical analysis. The material properties are consistent with the results found in Section 4.1, besides the value from E which is taken from Cambridge University Engineering Department (2003). This is due to the possibility for error in the measurement, which is discussed more in Section 6.4. The data for the axial direction is used.

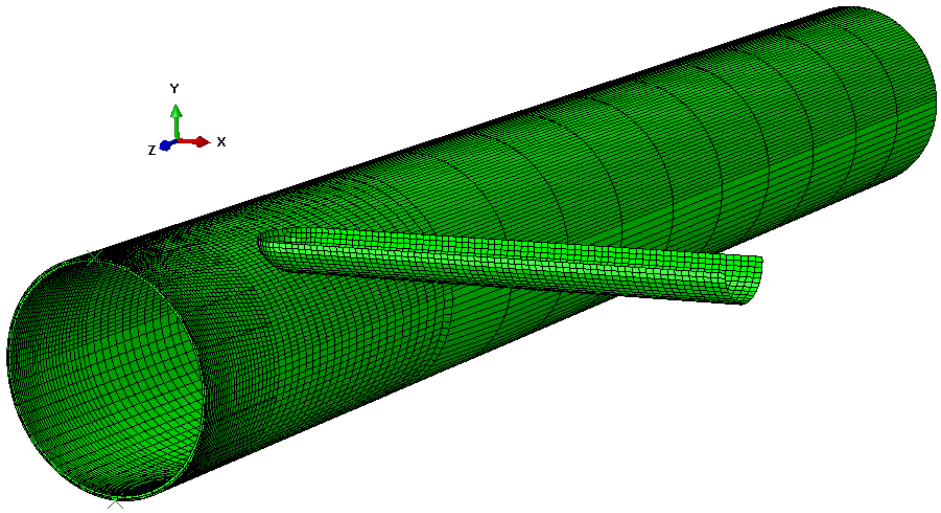

Figure 5.1: Global model with indenter 2

The material properties used in the numerical model are given in Table 5.1.

Table 5.1: Material properties

E [GPa]	σ_y [MPa]	σ_u [MPa]	ν [-]
210	347.47	399.49	0.3

The σ-ε_p curve for the material is shown in Figure 5.2.

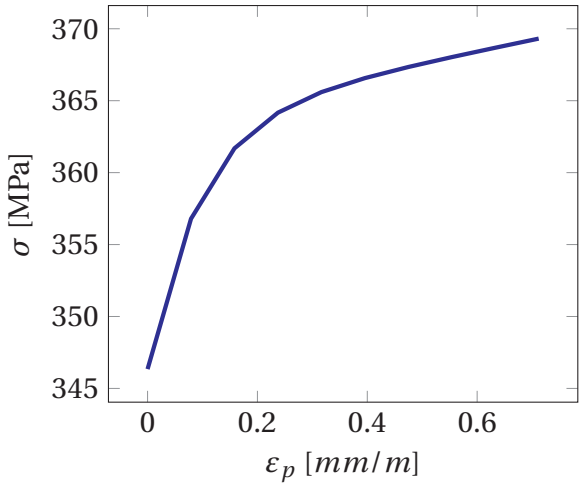

Figure 5.2: σ-ε_p for the material

5.3 Boundary condition and loading

There are several boundary conditions applied to the pipeline. A closed edge is modelled by using a end cap of shell elements on the end. The pipeline has symmetry in the transverse plane. The pipeline is restrained in all directions for the pipe end. The clamp simulates the block, restraining movement at the part of the pipe for the indention process.

The analysis was done in two parts, with quasi-static loading. First an elastic-plastic analysis with denting the pipe, creating the deformed pipe geometry. The dent depth is taken from the experimental work. The second part is an elastic analysis, where internal pres-

sure was applied with different levels of pressure, similar to the pressure graphs in Figure 4.10. The deformed mesh from the first part was imported for the second part, and do not take account the residual stresses and strains due to plastic deformation during the denting process.

5.4 Results

A contour plot of the stresses in the dent is shown in Figure 5.3 for the model. Here from the case with indenter 3, at the end of the first part of analysis.

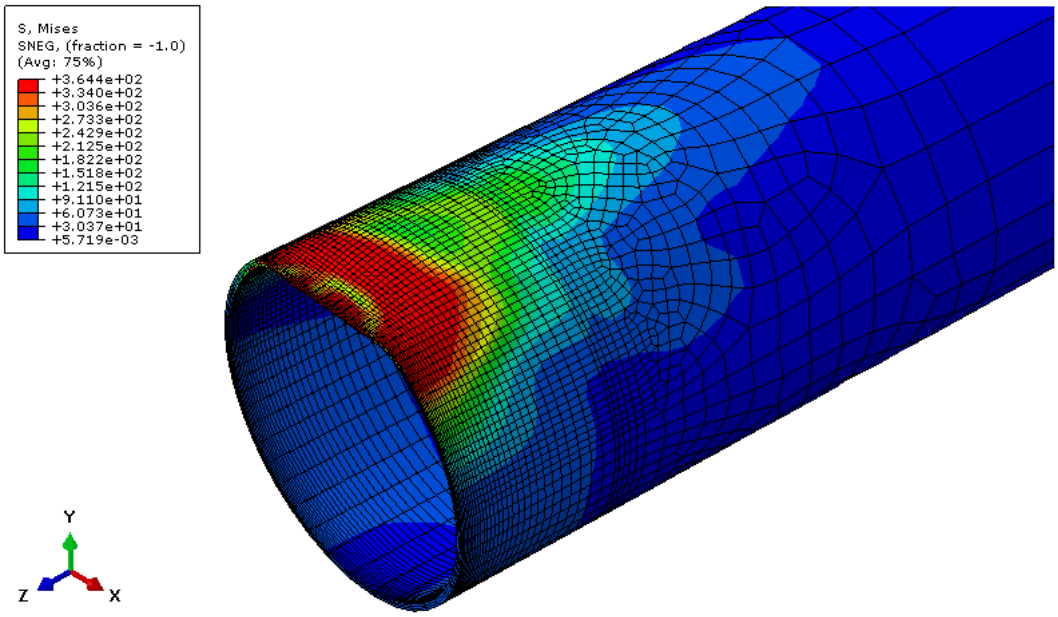

Figure 5.3: Stresses in the global model

Chapter 6

Discussion

The results from experimental and numerical work is evaluated and discussed. It should be noted that second run of the experimental work was a improved from the first run by taking the pressure down to 0 bar in between the pressure levels. This made the the result from dent I difficult to compare with dent II-IV in some cases.

6.1 Dent geometry

The results from the numerical model before the internal pressure is applied and compared with the results from the 3D acquisition methods. Both the ATOS optical 3D scanner and the Autodesk 123D catch app was used for dent I. By evaluating the resulting 3D model it was found that a higher precision archived by using ATOS optical 3D scanner. ATOS optical 3D scanner used structured light to obtain the measurements of geometrical distances, hence the model was scaled 1:1. When the app was used, a 10 mm times 10 mm sticker tape was used to scale the model up to correct size, which is a possible source for errors. Furthermore, it was concluded that Autodesk 123D catch app was less time consuming and gave good enough results for this study, therefore was used on all the dents and presented here. Figure 6.1 and 6.2 depicts the geometry of the dent in the YZ- and XZ-plane, according to the coordinate system in Figure 4.13.

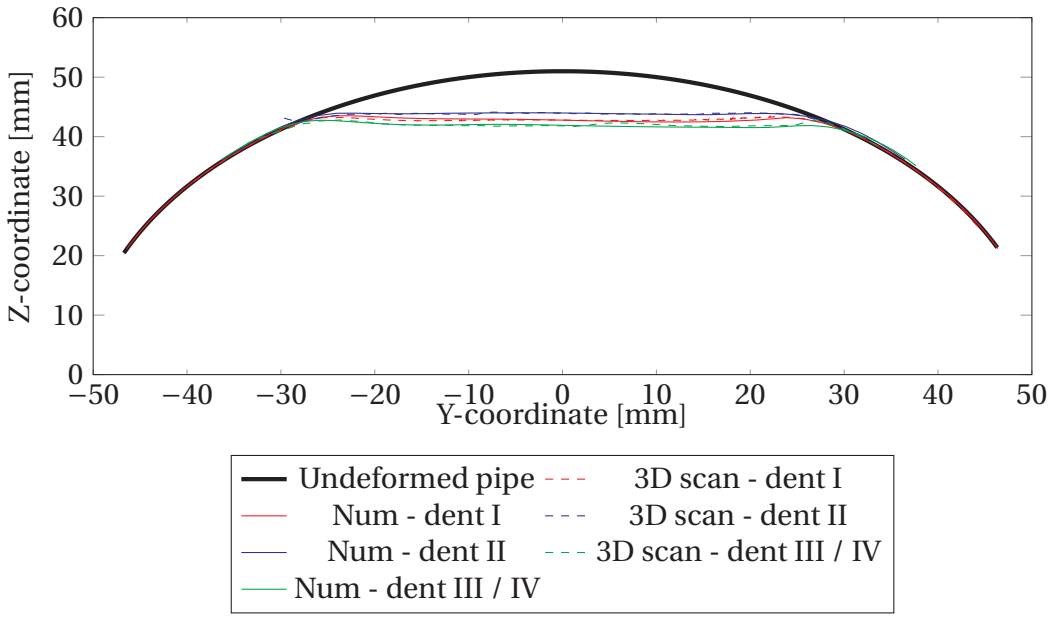

Figure 6.1: Dent in YZ-plane

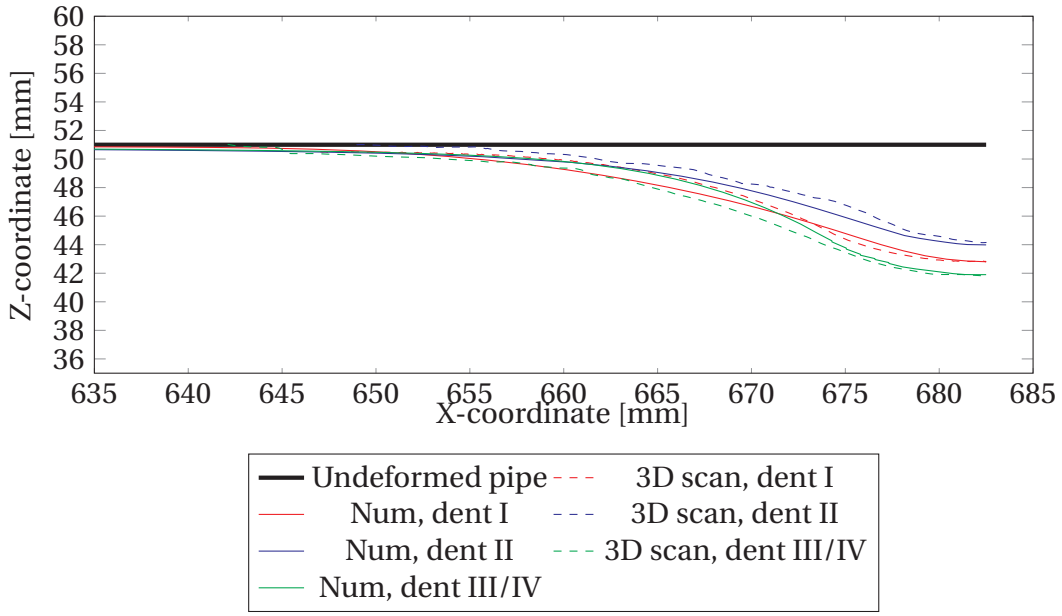

Figure 6.2: Dent in ZX-plane

The geometry is plotted in two dimensional (2D) where the origo is located in the centre of the dent. The dent is assumed symmetrical around the z-axis, hence only half of the dent is plotted in XZ-plane. It is compared with the undeformed pipe and the deformed numerical model for the three different dent geometries.

The two plots shows good correlation in YZ-plane with regards to dent geometry. It should be noted that the dent geometry varies little between the different geometries, except for the dent depth with regards to the YZ-plane when x = 0 mm. The difference is more significant for the short side of the dent (XZ-plane). A reason is that the 3D acquisition tool has difficulties scanning the slope of the dent wall, hence creating the uneven plot for the 3D scan. This was a problem for both 3D acquisition tools. It should be noted that the dent I and II seem to have similar shape, which is unexpected as dent II and III have more alike shape of the indenter's. In addition, by physical observations the geometry do not have the big differences in the center planes, but in the overall shape of the dent. This can be seen in Figure 4.8. A limitation of the 3D acquisition tool is the sensitivity to glare from the material, which created difficulties for obtaining the correct geometry. Measured was taken by painting the surface with matte paint, this improved the scanning however could still be a source of error. It was also added reference points to further improve the scan.

There were some differences between the physical dent and the numerical one. One of the significant is caused by the shape of the indenter and how it indents the pipe samples. The indenter's was made to order so it would fit into the test block for the denting process with a diameter of 29 mm. The indenter was however not made exactly as ordered, hence having a smaller diameter than the test block inlet. This deviation from the drawing allowed it to move when denting. Meaning the indenter had a straight heading when going in, then tilting when the penetration of the pipe started. This left the final dent with a small angle in the radial direction and not being straight as it was intended. It should be noted

that the angle was not so significant that it appeared in the 3D model. Another interesting observation was made when the dent was introduced on the pipe samples, the indenter pushed the material to the end of the dent leaving a small edge with the excess material. Figure 6.3 shows the phenomena on dent IV. These deviation from expected theory made it difficult to accurate create a numerical model that would depict the experiments in a good manner.

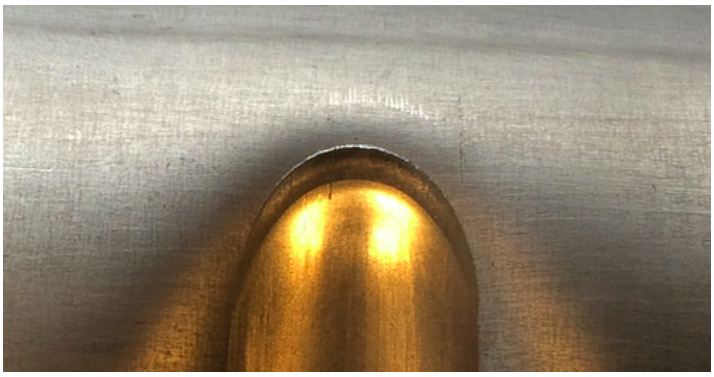

Figure 6.3: Excess material on dent tip

6.2 Rerounding

The variation in dent depth from the experimental work as shown in Figure 6.4, depicts that the rerounding effect discussed in Chapter 2.3. The most notable to see in the graph is that the difference between the dent without a gouge compared with the others which contains a gouge. It is more "rerounded" than the others. Maxey as cited in BMT Fleet Technology (2012) writes about that the combined dent and gouge shows less recovery to original shape compared to a plain dent, which is consistent with the graph presented. The relative difference between the two dents that has the same geometry is measured to be 0.6 mm. Indenter 2 and 3 has a similar geometrical shape, both for the indenter tool and the dent. The loading applied to the test sample is different, however the maximum change in dent depth and final dent depth is comparable between the two. The plot indi-

cates that the rerounding behaviour is similar regardless of the initial geometrical shape, and suggest that the rerounding behaviour could be dependent on material properties and not geometrical shape.

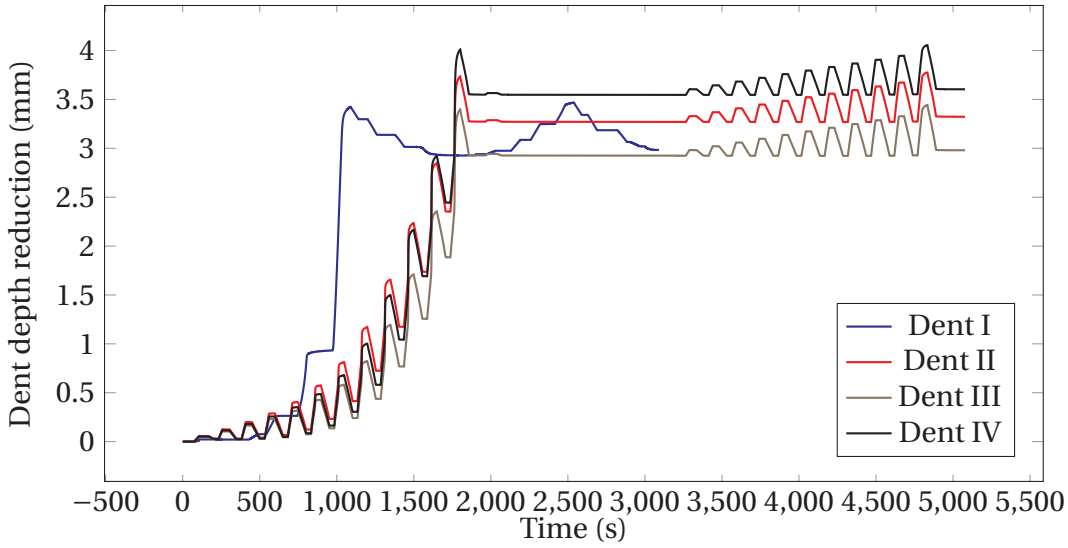

Figure 6.4: Dent depth

The dent depth is compared with the numerical analysis to see how well it predicts the dent depth. Now the pressure is plotted against dent depth, and Figure 6.5 shows how the dent depth varies without including the removing of pressure in the experimental results. They are compared with the numerical analysis. Figure D.1 and D.2 shows the experimental results for dent II, III and IV with how rerounding works with removing pressure between each step. They are found in Appendix D. The numerical analysis presented below is a elasto-plastic analysis run straight after the denting described in Section 5.3, hence when the residual stresses are still acting on the pipe.

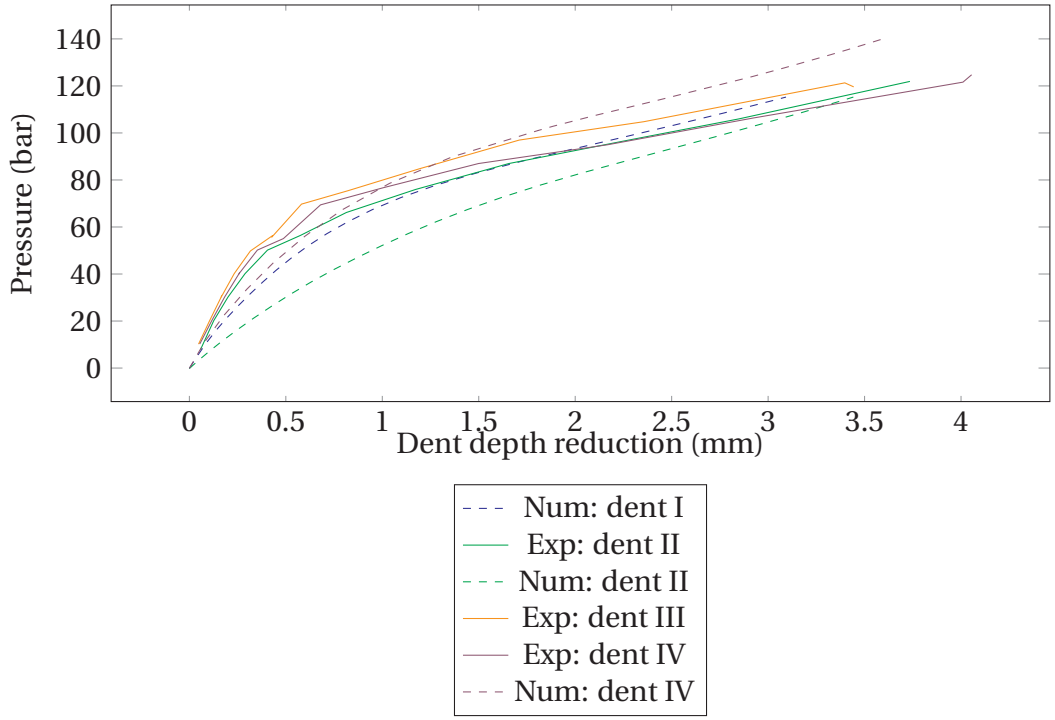

Figure 6.5: Dent depth versus internal pressure

From the graph above some conclusion might be made, however it should be noted that the amount of data is to little to say anything certain. The numerical model shows compliance with the experimental work, with a more theoretical behaviour. What is meant by theoretical is that it increases with a smooth behaviour, whereas the experimental work has a more uneven curve which can be due to the uncertainties around the experimental work.

An observation that was made that even if the initial geometry had seperate geometries, after rerounding the dent's became more alike. Hence the amount of rerounding contributes a noteworthy change towards one type of geometry. This may be a indication that it do not matter how the dent looks before pressure, since it will reround to a "common" dent shape.

The rerounding effect may be the reason for a variation in the position of the cylinder in the experiments, which created the loading on the pipe sample. Figure 6.6 shows the cylinder position over time. This is due to the increase of the internal volume in the pipe due to the dents experiences the rerounding effect. Therefore it can be seen in the strains obtained from the experimental work that they do not go back to zero when a low load as expected in the linear area in the ε-σ curve. The starting zero level is showed with the black dashed line in the plot. In compliance with the rerounding shown above, the magnitude of the effect is smaller for the second cycle. It should be noted that this effect can also be caused by leakage in the system, however no obvious leak was observed during testing.

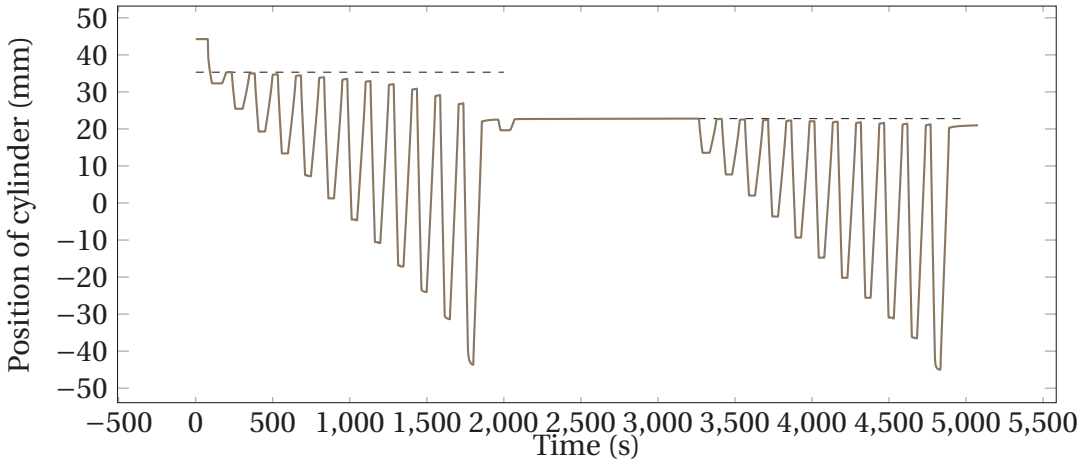

Figure 6.6: Cylinder position during run 2

6.3 Stress concentration factor

The SCF was estimated according to Chapter 2.2. The SCF was then compared between experimental and numerical results. It should be noted that all the numerical results has no gouge, whereas the experimental results contains a gouge except dent IV. The challenges around comparing the numerical model and experimental model is discussed.

6.3.1 Challenges and procedure

There were challenges for creating a numerical model that would predict sufficient results that could be verified with the experimental model with regards to SCF. The underlying issue was when the strain gauges was introduced to the dents. During the indention process the pipe sample is exposed to a loading (indention) and deload, such as the spring back effect mention in Chapter 2.3. The pipe sample have reached yield and the dent has a permanent deformation. Hence there is residual stresses in the pipe sample which is hard to obtain. If the strain gauges had been applied in the indention process, they would most likely be damaged during it. Therefore the strain gauges was applied after, and the assumption that there is no residual stresses in the material is a great simplification to the problem. The strain gauges also reached saturation when the internal pressure was applied at different pressure levels.

The information available from the experiments showed some non-linear material behaviour. In order to predict SCF von Mises was used as a combined stress criteria, which is based on Hooke's law as discussed in Chapter 2.1.1. This has the underlying assumption that the material has a linear behaviour which is not the case for the strain gauges placed in the dent for the first round of internal pressure. There are methods to predict combined stresses for strains in the non-linear part of the material curve, however these are to complicated for this study. A alternative is also to used strain based assessment, as discussed by Noronha et al. (2010) amongst others. The method is part of ASME codes, and would allow a greater range of dented pipelines to be considered safe. However the method raises some questions with regards to the equations and demands great caution to the representation of the pipe geometry.

Therefore a procedure with assumptions is used to predict and compare SCF from both

numerical and experimental work. According to Pinheiro et al. (2014), evidence based on experimental and numerical work can prove that dented steel pipes under cyclic internal pressure deforms elastically after the first cycle if the maximum pressure is not increased. This observation is also made in Figure 6.4 for the dent depth, the material goes back to the starting position for the second cycle of loading. Hence a linear material model can be assumed in order to calculate SCF. Since several of the strain gauges reached saturation when closing to yield stress, the SCF was found for the dent geometry when it is pressurized up to 10, 50 and 110 bars. The following procedure is similar for the numerical and experimental work. The loading is done as in Figure 4.10 up to the first time it reaches 10, 50 and 110 bars respectively. Then the geometry at that point is "exported" and a clean pipe sample/numerical model without residual stresses is assumed. Now there is three models to work with from both the numerical and experimental work. The procedure for the 10 bar model is explained. For the other two the procedure is similar with 50 and 110 bars instead. A simple linear elastic analysis is run on the numerical model with pressure up to 10 bars, and the SCF is then found. For the pipe sample in the experiments, the strain history is cleaned, giving a strain curve starting at 0 and gives the linear strain curve pressurized up to 10 bars respectivly. By assuming Hooke's law and utilizing von Mises stresses the SCF is found. The result and comparison is presented in the following section.

6.3.2 The 10, 50 and 110 bar model

The SCF compared with numerical analysis for dent III and IV in all three cases with experimental work. Figure 6.7, 6.8 and 6.9 for the 10, 50 and 110 bar model respectively. They depicts the SCF plotted against pressure in % of σ_y.

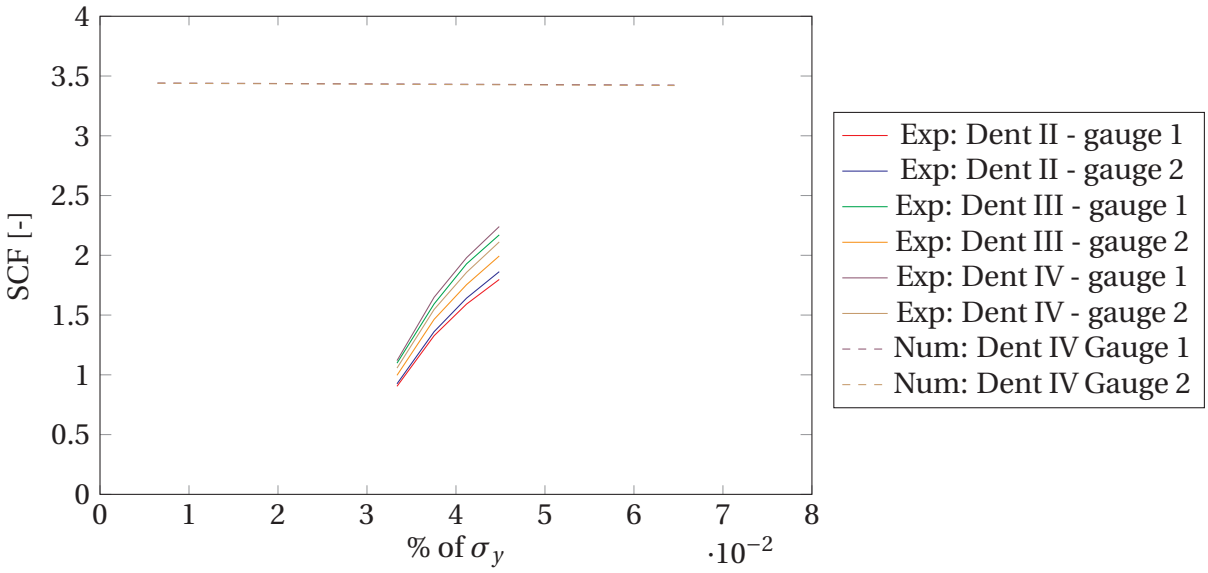

Figure 6.7: SCF for experimental work and numerical work at the 10 bar model

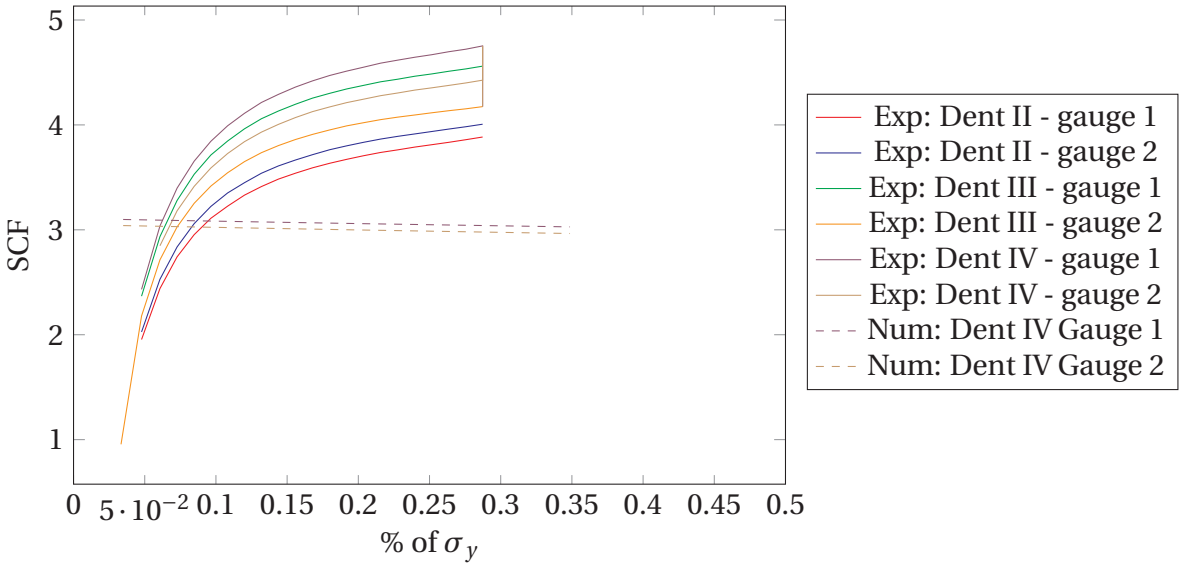

Figure 6.8: SCF for experimental work and numerical work at the 50 bar model

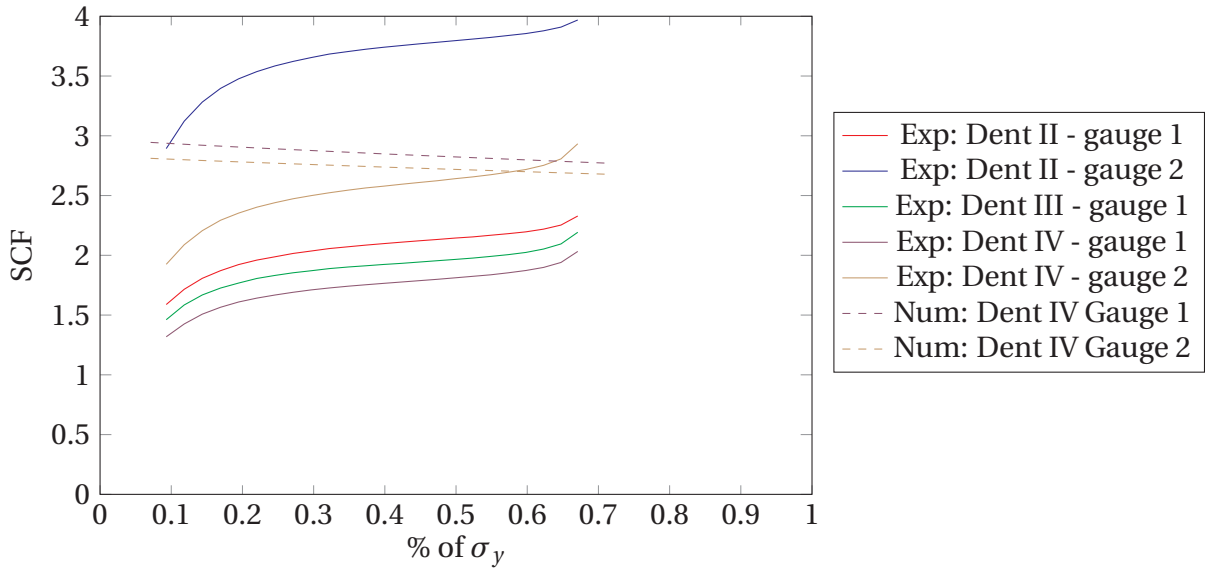

Figure 6.9: SCF for experimental work and numerical work at 110 bar model

For the 10 bar model, is the steps between the points are few, hence the slope is steeper compared to the other two models. The 50 bar model is presented in Figure 6.8. It can be seen that all the gauges has a similar development regardless of shape. Another observation is that the location of the gauges do not correspond to the amount of stress as expected, as strain gauge 2 for dent II had a higher SCF than gauge 1. The strain gauges was located were the highest stress was expected, hence strain gauge 1 was expected to have the highest SCF. It is interesting to see how dent IV, which is a plain dent, has a higher SCF than the other dents that contains a gouge.

For the 110 bar model, the same observations can be made as for the 50 bar model. In addition dent IV the results shows that gauge 2 has a higher SCF than gauge 1. For dent II, gauge 2 shows especially high values. The reason is unknown for the author, however it questions the location of the gauge based on numerical predictions and it might not be located on the maximum strain in the dent. Therefore the result should be used with care.

It is hard to say something certain regarding the impact from geometry on SCF. Dent II seems to have the lowest values in the earlier stages of rerounding (10 and 50 bar model) then becomes the dominating dent. The higher pressure applied to the pipe sample creates a more spread results.

The graph also include the results from numerical model, which are plotted with dashed lines. It shows low correlation between the numerical model and the experimental work. The slope for the numerical model is negative and linear whereas the experiments increases with a non-linear shape. This means that the von Mises stresses increases more rapid than the internal pressure for the experimental work, where the numerical work the von Mises decreases with respect to internal pressure. The biggest challenge of the numerical part is the simplification of the model. There are some assumptions that are taken, as creating a realistic environment for a numerical analysis is challenging. However the most significant difference is that the numerical model do not contain the gauge, only the dent. Therefore it should have coincided with dent IV. It is difficult to accurately describe all the factors that affect the experimental model in a numerical model. Contact is hard to model numerically, and has been a challenge for this study. A possible improvement is to run a explicit version of ABAQUS, however this is a time consuming process.

6.4 Limitations and sources of error

The results and method are prone to errors and limitations. The material testing could have been improved with using two extensometer instead of one, placing one on each side of the test specimen. Using the mean value would eliminate the bending stress. The bending stress is due to the test specimen for radial direction was straighten out before testing, therefore a significant amount of bending stress would appear for low stresses.

This would mean that the result are inaccurate in the start of testing, then the error will decrease when the stresses is increased and the specimen is straighten. When reaching yield the result would be accurate and therefore the value for yield stress could be used and the E could be inaccurate. Therefore the tabular value for E was used instead of the one calculated from material testing. Chen et al. (2016) have found out that E do not unload linear, it shows significant curvature and hysteresis. The mechanically-measured E has also been measured to be consistently lower than the E measured physically, especially after plastic straining. Ghaei et al. (2015) also talks about how E experiences hysteresis and the effect should be considered when springback is involved. This effect should have been included to further improve the numerical model, however the present study was limited due to time.

For the experimental work, some improvements and errors are described. Using a block in the indenter process is not a realistic case. It is a strict way do penetrate the pipeline, as it is indentation is not forced in the same matter on a pipeline locked in all directions besides one. It also made the contact hard to model in the numerical model. The strain gauges did not measure all the information as the range was larger than expected. In hindsight strain gauges that can handle larger strains should have been used. The disadvantage is that it is difficult to obtain strain gauges that will measure in three direction and also take large strains. The three directions are necessary to get look at the combined stress. Therefore strain gauges with one direction should have been considered. Also the placement of strain gauges was based on numerical analysis for a dent without a gouge, and the results for SCF implies that there might be other locations with higher strains. This is due to that strain gauge 2 showed higher values in some cases, where strain gauge 1 was the one supposed to measure the highest strain in the dent. The reason for not accurately describe the gouges was that the geometry of the gouge was not of interest, but the dent geometry in general. However, a improvement would be to measure the gouge and include it in the

numerical result to obtain a more correct model.

Chapter 7

Conclusion

The aim was to evaluate current assessment methods, and investigate the impact the dent geometry has on SCF. The most common assessment method is presented in Cosham and Hopkins (2006), based on EPRG methods. However, this is a very conservative approach, and most of the standards do not allow the combined damage of dent and gouge.

It can be concluded that the numerical model needs further improvement and cannot be used to estimate SCF for dent with gauge. It showed good correlation with the indention process, nevertheless there was several issues with predicting the non-linear behaviour of the material to estimate SCF and compare it with the experimental work.

The experimental work showed that the strains in the dents are so high that there was issues with the strain gauges, leading to saturation. From the strain gauges that did not fail, some concluding remarks could be done. For indenter 1 the SCF was lower compared to indenter 3 early in the rerounding process, then becomes significant larger compared to the other strain gauges. However the results should be used with care, as there is indications that there are other areas in the dent with higher strains. Furthermore, a test method is created in order to evaluate SCF and fatigue life, with suggestion of how to improve it.

Chapter 8

Future work

The ground work has been laid for further experimental work around the topic of the combined damage with dent and gouge. To avoid saturation of the gauges the use of one direction strain gauges with higher range should be used to predict strains.

Some other suggestions for topics to continue the investigations are

- Measurement of residual stresses in the dent.
  The residual stresses left in the pipeline after dented should be further investigated.
- Fatigue life predictions
  There is little information about how the combination of the plain dent and gouge affects the fatigue life. Fatigue life analysis could be carried out to investigate how a gouge impacts the plain dent.
- The impact of dent geomtry on SCF
  This can be done by different factors as suggested by Alexander (1999) in Section 1.5.

Bibliography

ASME (1992). *Liquid Transportation Systems for Hydrocarbons, Liquid Petroleum Gas, Anhydrous Ammonia, and Alcohols: ASME B31. 4*. ASME.

EGIG (2016). 9th EGIG report on gas pipeline incidents. Technical report.

Georgia Institute of Technology (2000). Ae3145: Strain transformation and rosette gage theory.

Alexander, C. and Jorritsma, E. (2010). A systematic approach for evaluating dent severity in a liquid transmission pipeline system. In *2010 8th International Pipeline Conference*, pages 811–818. ASME.

Alexander, C. R. (1999). Review of experimental and analytical investigations of dented pipelines. *ASME-PUBLICATIONS-PVP*, 395:197–210.

Alexander, C. R. and Kiefner, J. (1997). Effects of smooth and rock dents on liquid petroleum pipelines. In *1999 API Pipeline Conference, Dallas, Texas*.

Allouti, M., Schmitt, C., and Pluvinage, G. (2014). Assessment of a gouge and dent defect in a pipeline by a combined criterion. *Engineering Failure Analysis*, 36:1–13.

ASME (2014). Gas transmission and distrubution piping systems. B 31.8, The American Society of Mechanical Engineers, New York, USA.

Berge, S. (2006a). *Compendium in Fatigue and Fracture Design of Marine Structures*, volume I. Department of Marine Technology.

Berge, S. (2006b). *Compendium in Fatigue and Fracture Design of Marine Structures*, volume II. Department of Marine Technology.

BMT Fleet Technology (2012). Dent fatigue life assessmen. Dot# 432 closeout report.

Cambridge University Engineering Department (2003). *Materials Data Book*.

Chen, Z., Gandhi, U., Lee, J., and Wagoner, R. (2016). Variation and consistency of young's modulus in steel. *Journal of Materials Processing Technology*, 227:227–243.

Cosham, A. and Hopkins, P. (2001). A new industry document detailing best practices in pipeline defect assessment. In *Fifth International Onshore Pipeline Conference Amsterdam, The Netherlands*.

Cosham, A. and Hopkins, P. (2006). The pipeline defect assessment manual. Technical Report 9909A-RPT-001 R1.05, The PDAM joint industry project, Newcastle, England.

Cunha, S. B., Pasqualino, I. P., and Pinheiro, B. C. (2014). Pipeline plain dent fatigue: A comparison of assessment methodologies. In *2014 10th International Pipeline Conference*, pages V002T06A041–V002T06A041. American Society of Mechanical Engineers.

den Haan, K. H. and Davis, P. (2014). CONCAWE oil and petroleum product pipeline performance review.

DNV (2014). Interference between trawl gear and pipelines. *Oslo: DNV*, (DNV-RP-F111).

Dowling, N. E. (1998). Mechanical behavior of materials: Engineering methods for deformation. *Fracture, and Fatigue, 2nd edition, Pretince Hall*.

Eliassen, L. (2007). Characterization of the mechanical properties of carbon anode materials. Master's thesis, NTNU.

Fish, J. and Belytschko, T. (2007). *A first course in finite elements*, volume 517. Wiley New York.

Ghaei, A., Green, D., and Aryanpour, A. (2015). Springback simulation of advanced high strength steels considering nonlinear elastic unloading–reloading behavior. *Materials & Design*, 88:461–470.

Hibbitt, Karlsson, and Sorensen (2001). *ABAQUS/standard user's Manual*, volume 1. Hibbitt, Karlsson & Sorensen.

Le Bastard, A. (2006). Influence of internal pressure for depth measurement on a dent. In *2006 International Pipeline Conference*, pages 135–141. ASME.

Noronha, D. B., Martins, R. R., Jacob, B. P., and de Souza, E. (2010). Procedures for the strain based assessment of pipeline dents. *International Journal of Pressure Vessels and Piping*, 87(5):254–265.

Ong, L., Soh, A., and Ong, J. (1992). Experimental and finite element investigation of a local dent on a pressurized pipe. *The Journal of Strain Analysis for Engineering Design*, 27(3):177–185.

Pinheiro, B., Pasqualino, I., and Cunha, S. (2014). Fatigue life assessment of damaged pipelines under cyclic internal pressure: Pipelines with longitudinal and transverse plain dents. *International Journal of Fatigue*, 68:38–47.

Race, J. M. (2008). Integrity assessment of plain dents subject to fatigue loading. Technical report, School of Marine Science & Technology, Newcastle University, Newcastle, England.

Rinehart, A. J. and Keating, P. B. (2002). Length effects on fatigue behavior of longitudinal pipeline dents. In *2002 4th International Pipeline Conference*, pages 1849–1858. ASME.

Roovers, P., Bood, R., Galli, M., Marewski, U., Steiner, M., and Zaréa, M. (2000). EPRG methods for assessing the tolerance and resistance of pipelines to external damage. *Pipeline technology*, 2:405–425.

Rosenfeld, M., Pepper, J. W., and Leewis, K. (2002). Basis of the new criteria in ASME b31. 8 for prioritization and repair of mechanical damage. In *2002 4th International Pipeline Conference*, pages 647–658. ASME.

Rosenfeld, M. J. (1998). Investigations of dent rerounding behavior. In *The 1998 International Pipeline Conference, IPC. Part 1(of 2)*, pages 299–304.

Shigley, J. E., Budynas, R. G., and Mischke, C. R. (2004). Mechanical engineering design.

Stone, R. (2012). Fatigue life estimates using goodman diagrams. *Retrieved August 2015*, 17.

Appendices

Appendix A

Raw data from experimental run 1

In the raw data the gauges are numbered from 0 - 3. All gauges are measured in $\mu m/m$

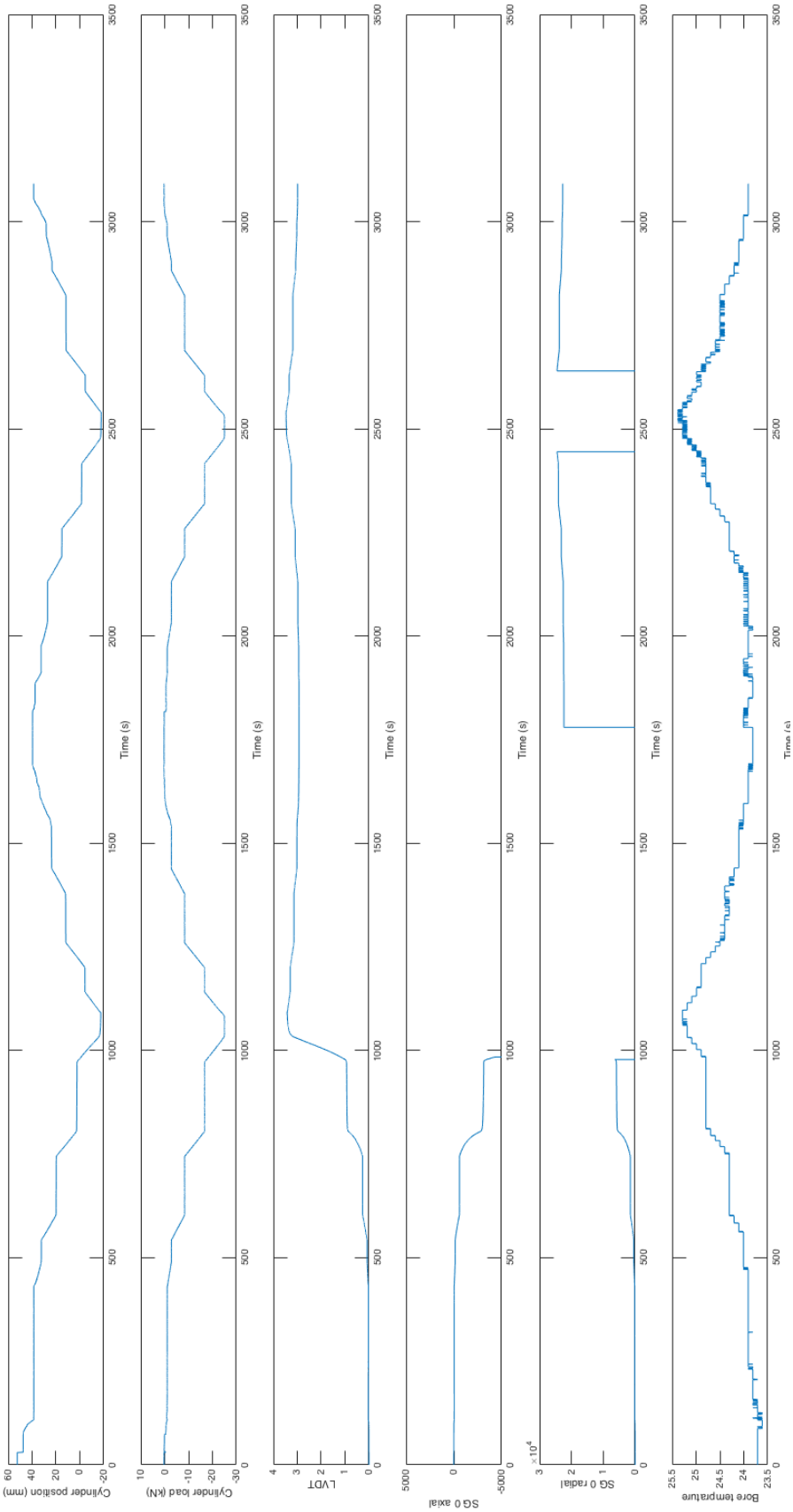
Cylinder position (mm)
Cylinder load (kN)
LVDT
SG 0 axial
SG 0 radial
Bore temperature
Time (s)

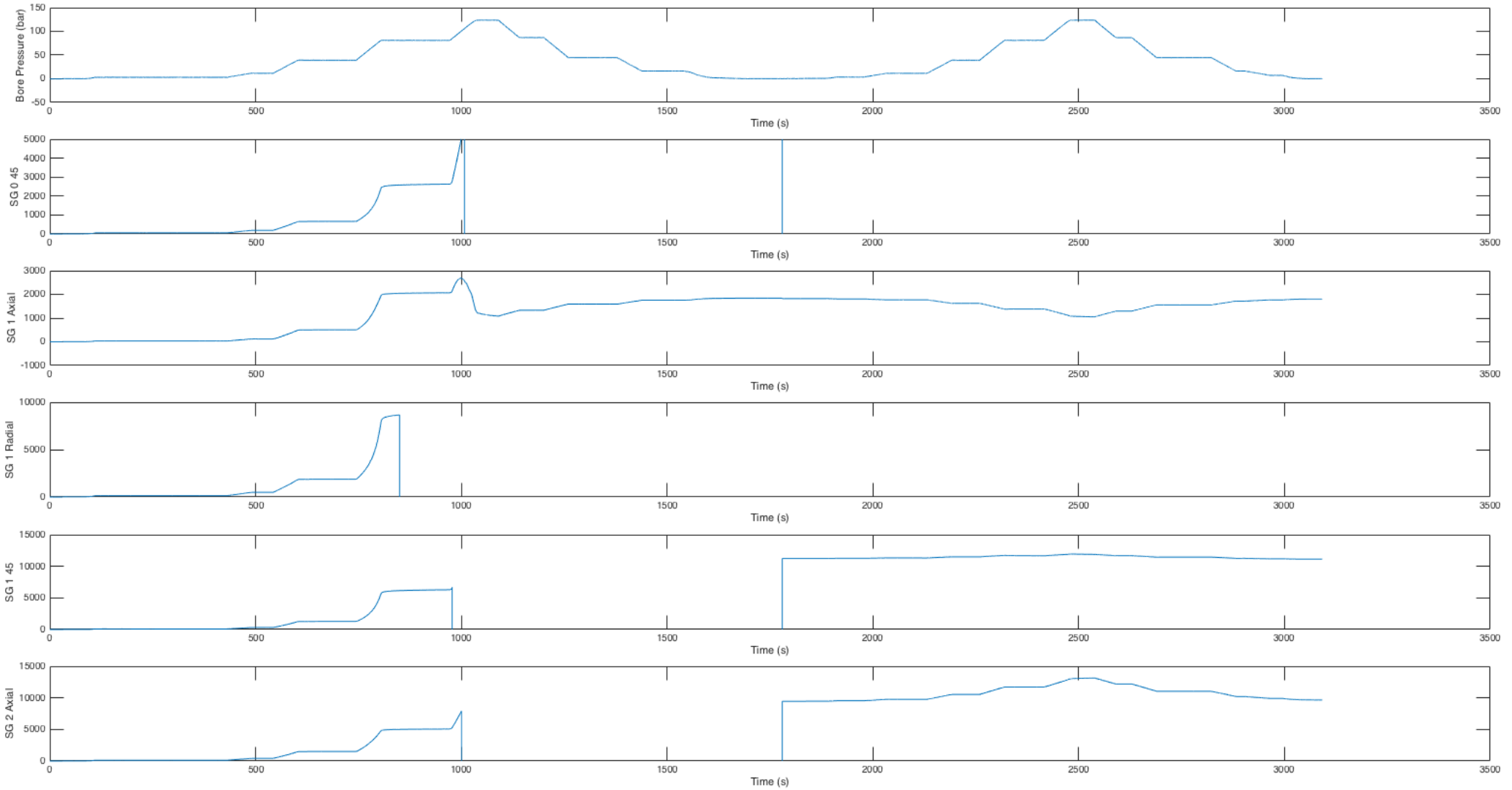
Bore Pressure (bar)
150
100
50
0
-50
0
500
1000
1500
2000
2500
3000
3500
Time (s)
SG 0 45
5000
4000
3000
2000
1000
0
0
500
1000
1500
2000
2500
3000
3500
Time (s)
SG 1 Axial
3000
2000
1000
0
-1000
0
500
1000
1500
2000
2500
3000
3500
Time (s)
SG 1 Radial
10000
5000
0
0
500
1000
1500
2000
2500
3000
3500
Time (s)
SG 1 45
15000
10000
5000
0
0
500
1000
1500
2000
2500
3000
3500
Time (s)
SG 2 Axial
15000
10000
5000
0
0
500
1000
1500
2000
2500
3000
3500
Time (s)

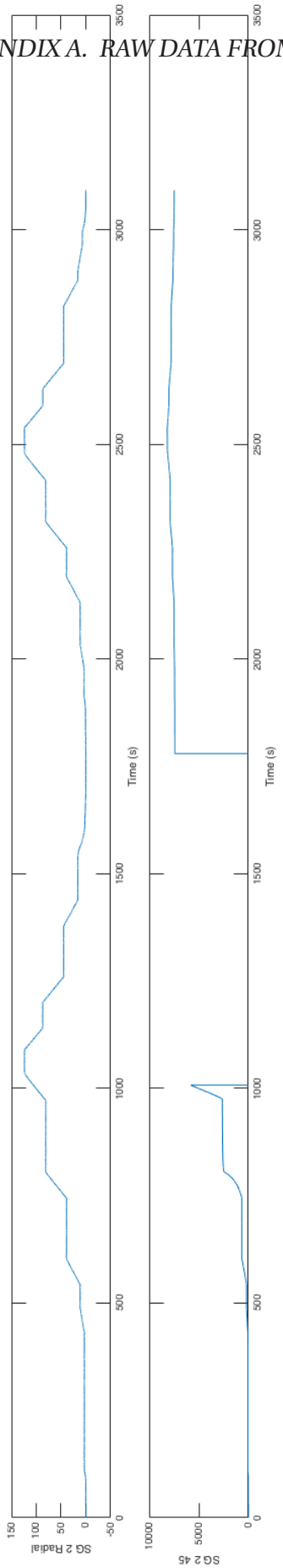
SG 2 Radial
150
100
50
0
-50
0
500
1000
1500
2000
2500
3000
3500
Time (s)
SG 2 45
10000
5000
0
0
500
1000
1500
2000
2500
3000
3500
Time (s)

Appendix B

Raw data from experimental run 2

In the raw data dent II is named A, dent III is B and dent IV is C. All gauges are measured in $\mu m/m$. Some of the gauges reached saturation, and showed a large negative value. The plot are corrected for those, hence the line goes out of range at some plots.

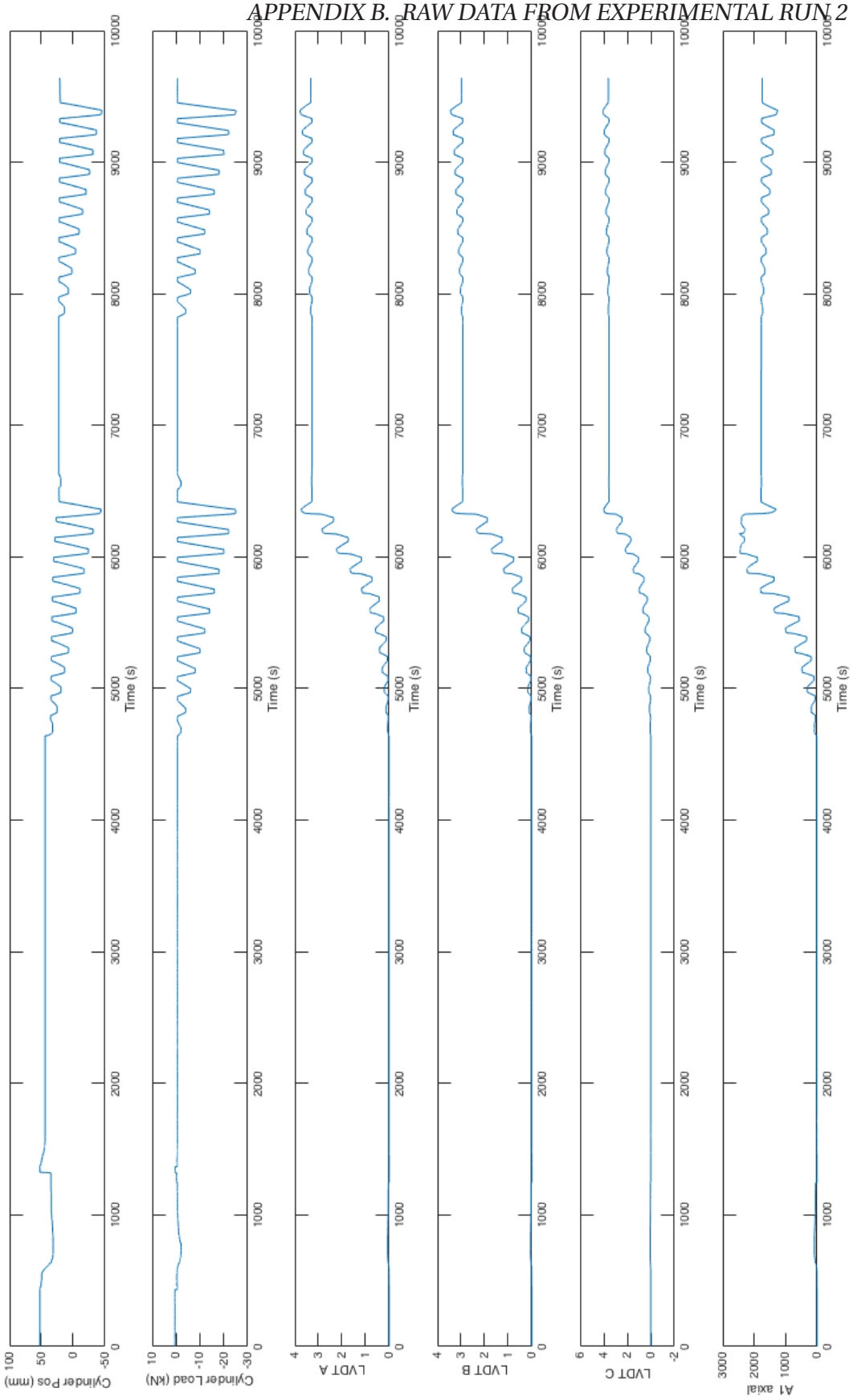
Cylinder Pos (mm)
Cylinder Load (kN)
LVDT A
LVDT B
LVDT C
A1 axial
Time (s)

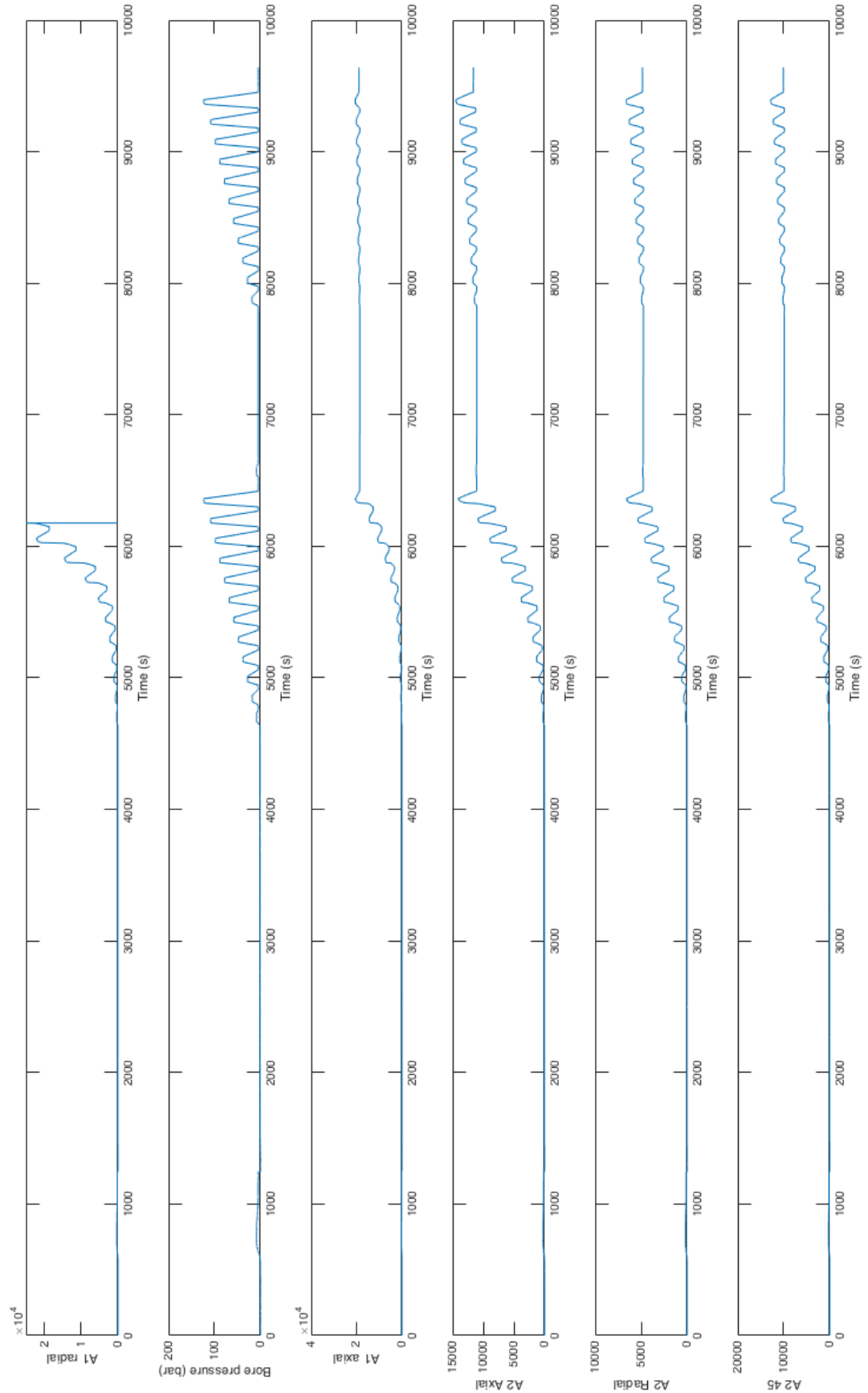
A1 radial
Bore pressure (bar)
A1 axial
A2 Axial
A2 Radial
A2 45
Time (s)

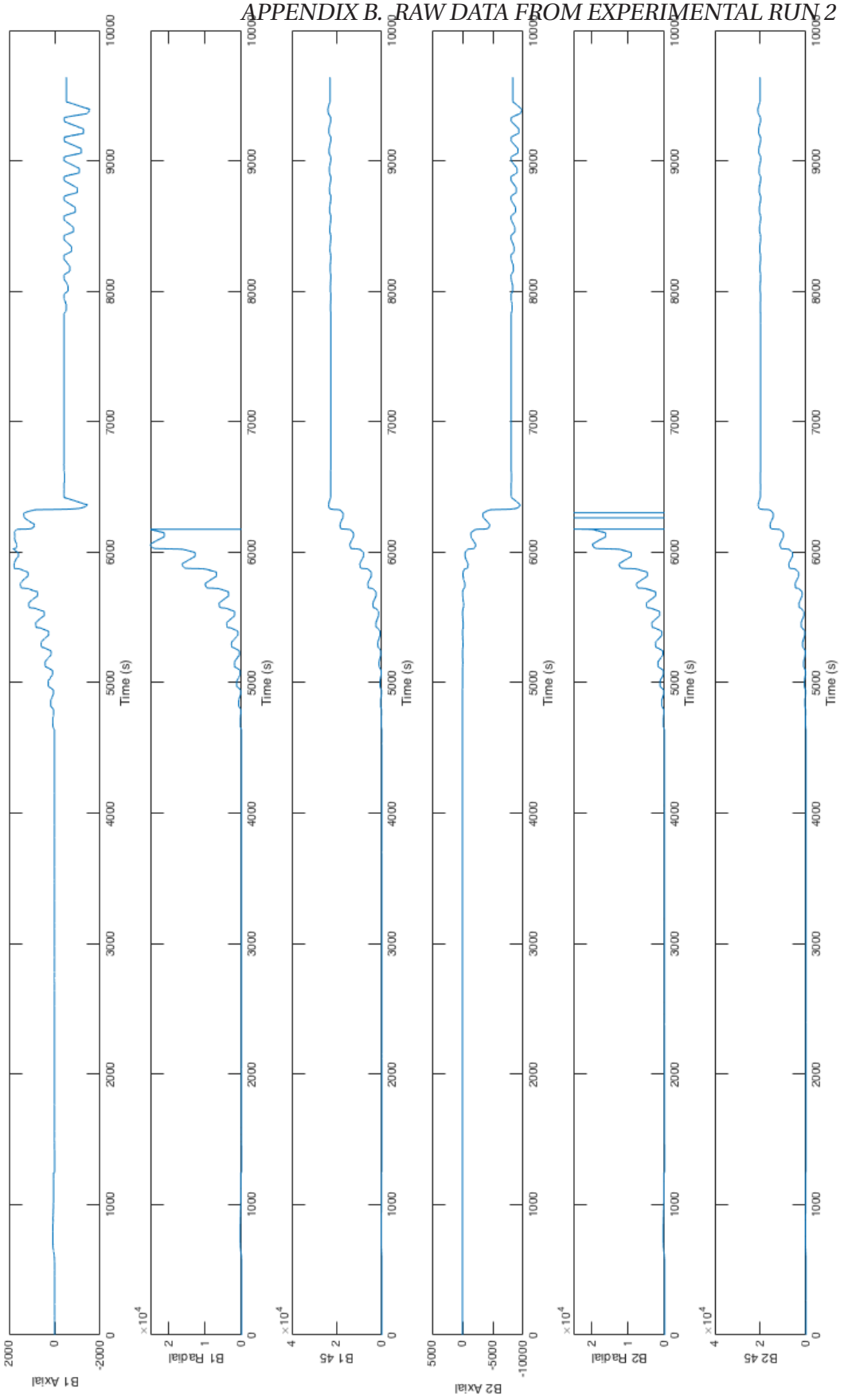
B1 Axial
B1 Radial
B1 45
B2 Axial
B2 Radial
B2 45
Time (s)

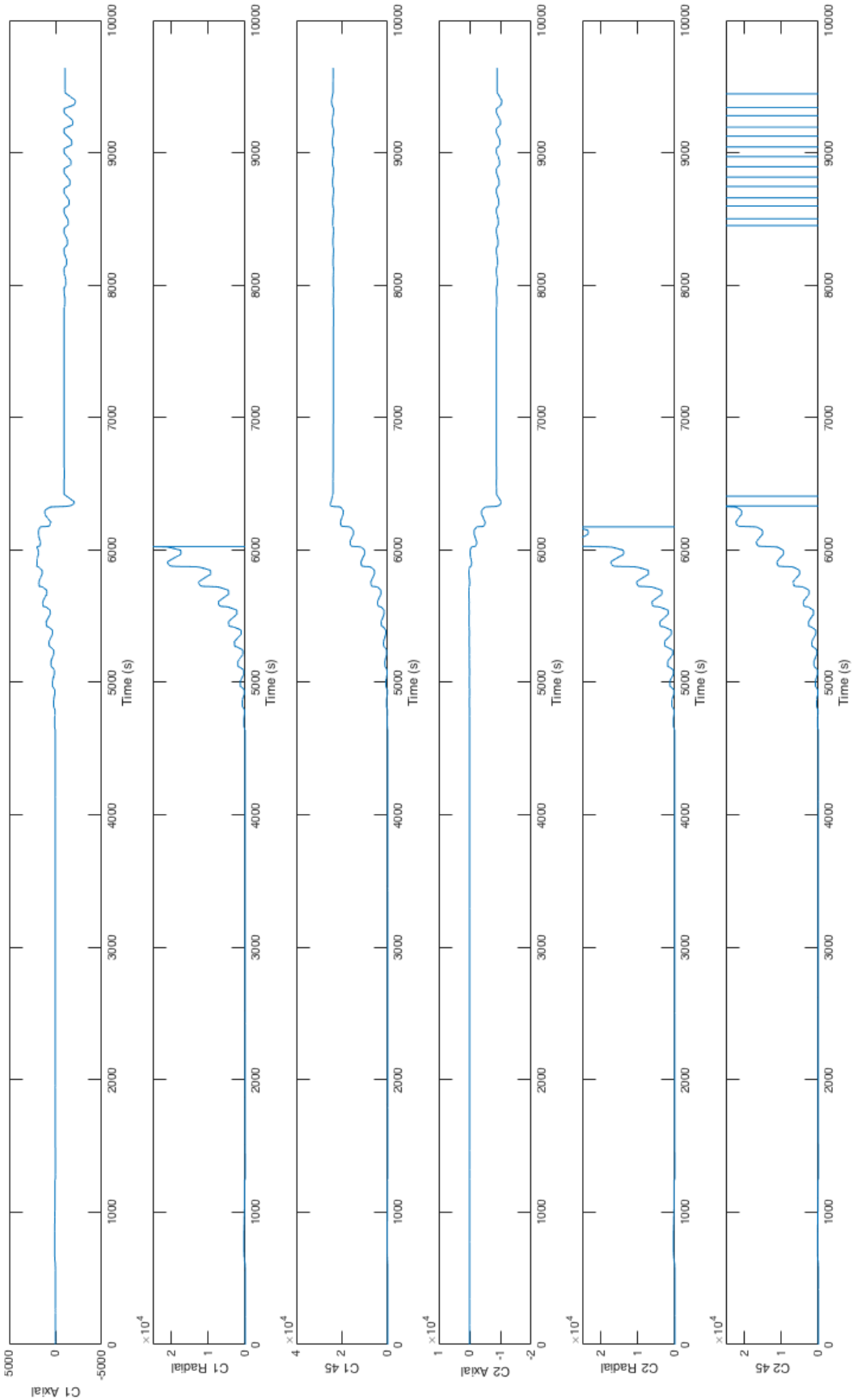
C1 Axial
C1 Radial
C1 45
C2 Axial
C2 Radial
C2 45
Time (s)

Appendix C

Raw data from experimental run 3

In the raw data dent II is named A, dent III is B and dent IV is C. All gauges are measured in $\mu m/m$

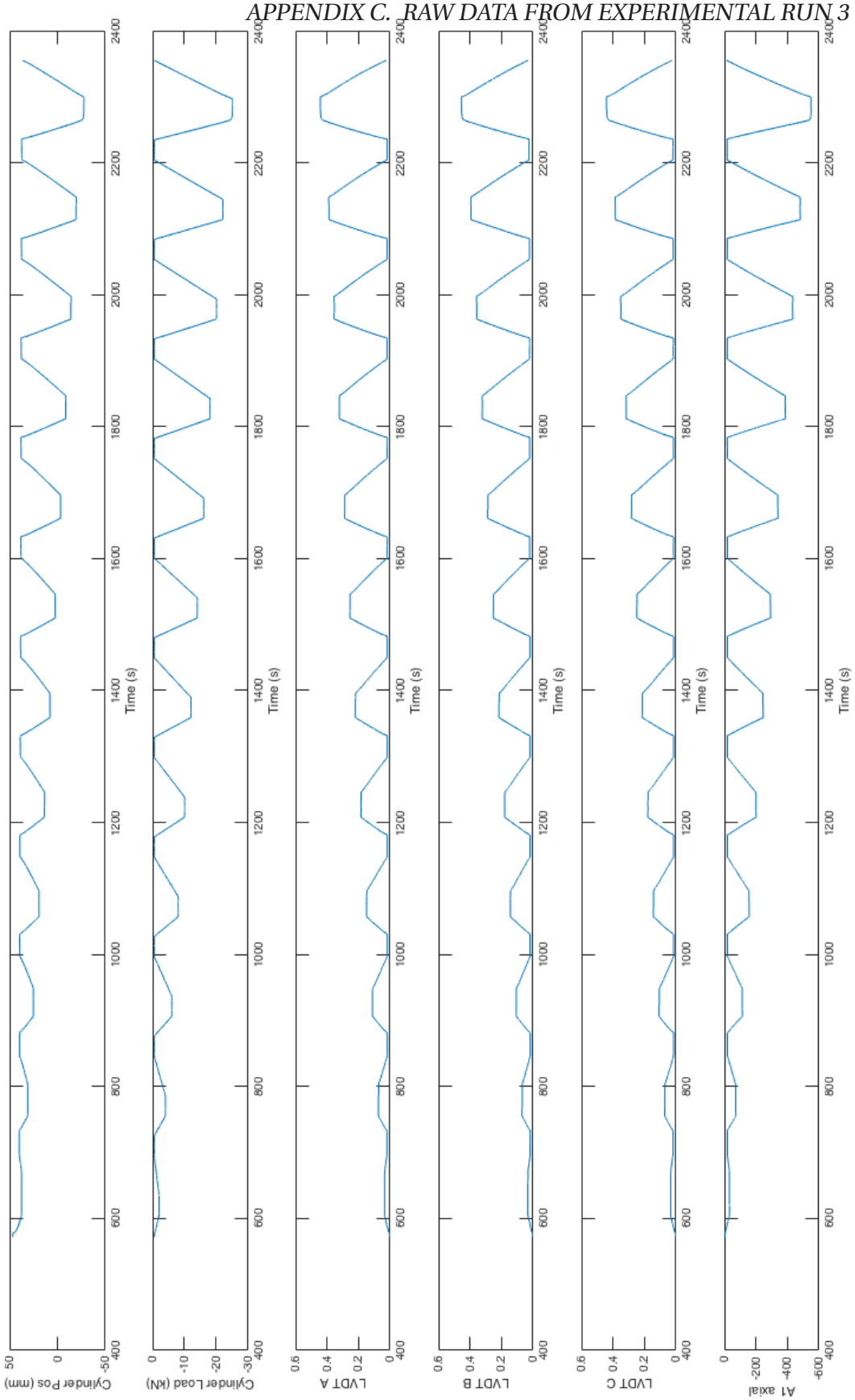
Cylinder Pos (mm)
Cylinder Load (kN)
LVDT A
LVDT B
LVDT C
A1 axial
Time (s)

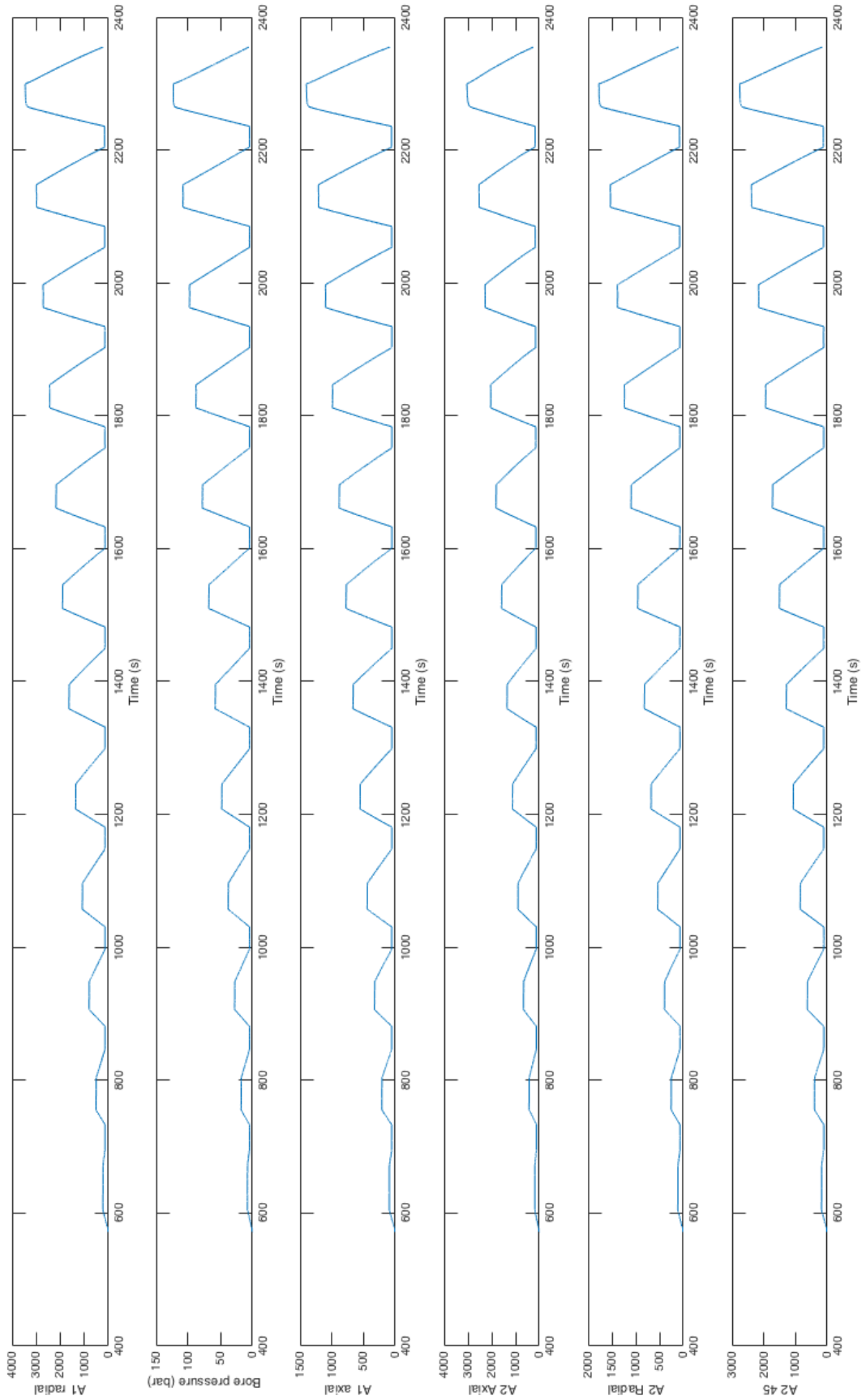
A1 radial
Bore pressure (bar)
A1 axial
A2 Axial
A2 Radial
A2 45
Time (s)

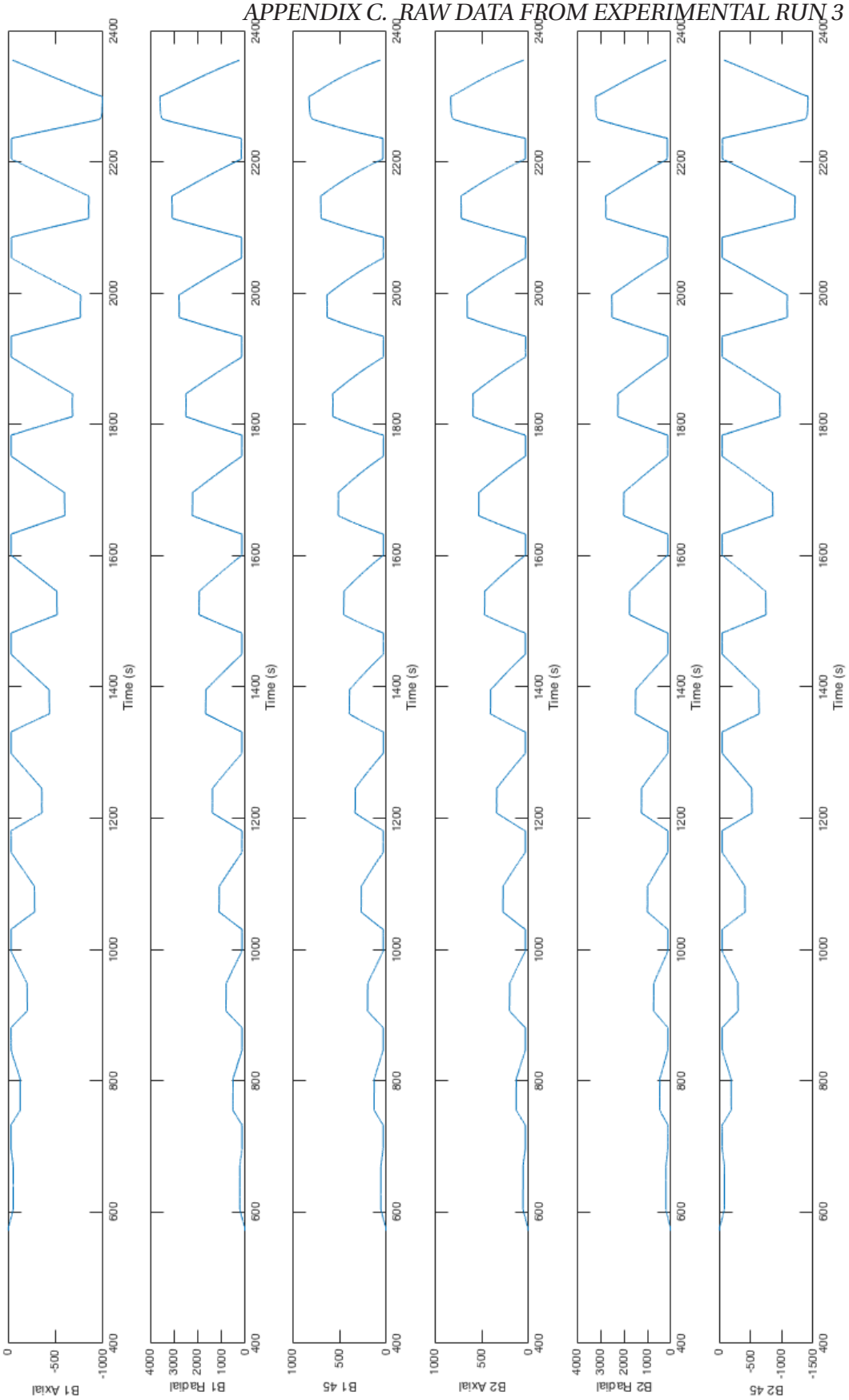
B1 Axial
B1 Radial
B1 45
B2 Axial
B2 Radial
B2 45
Time (s)

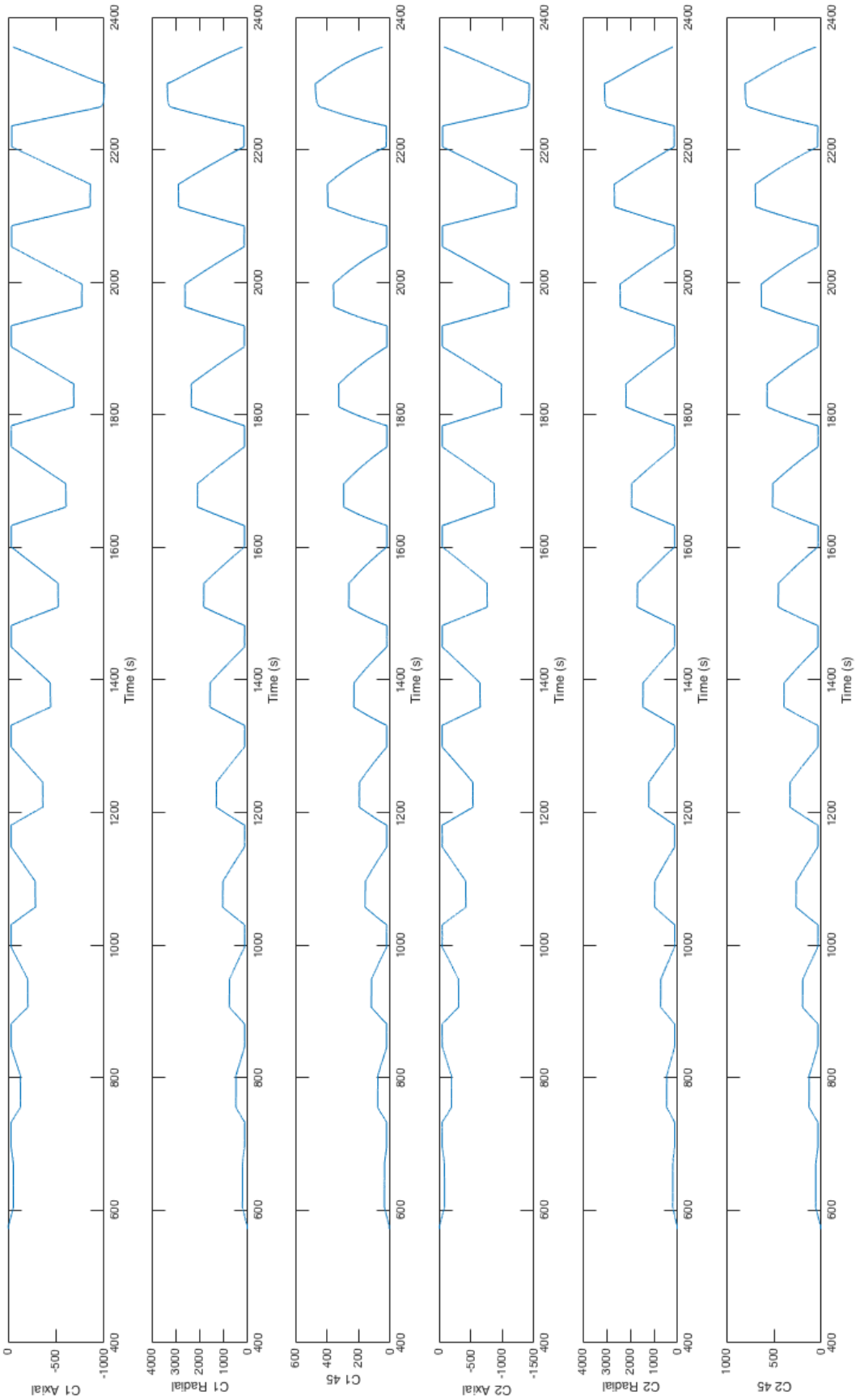
C1 Axial
C1 Radial
C1 45
C2 Axial
C2 Radial
C2 45
Time (s)

Appendix D

Additional results from experiments

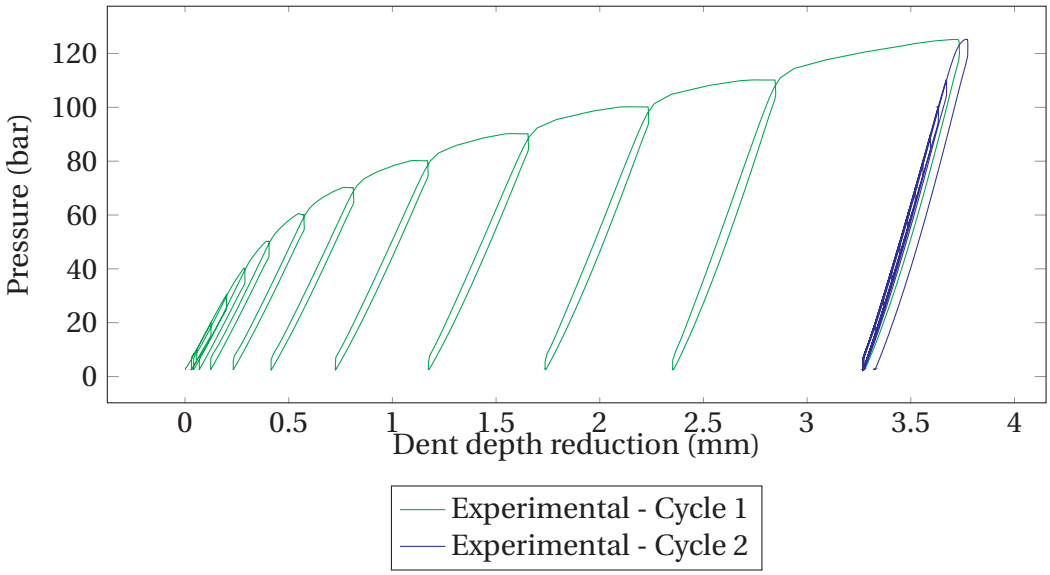

Figure D.1: Dent depth versus internal pressure for dent II

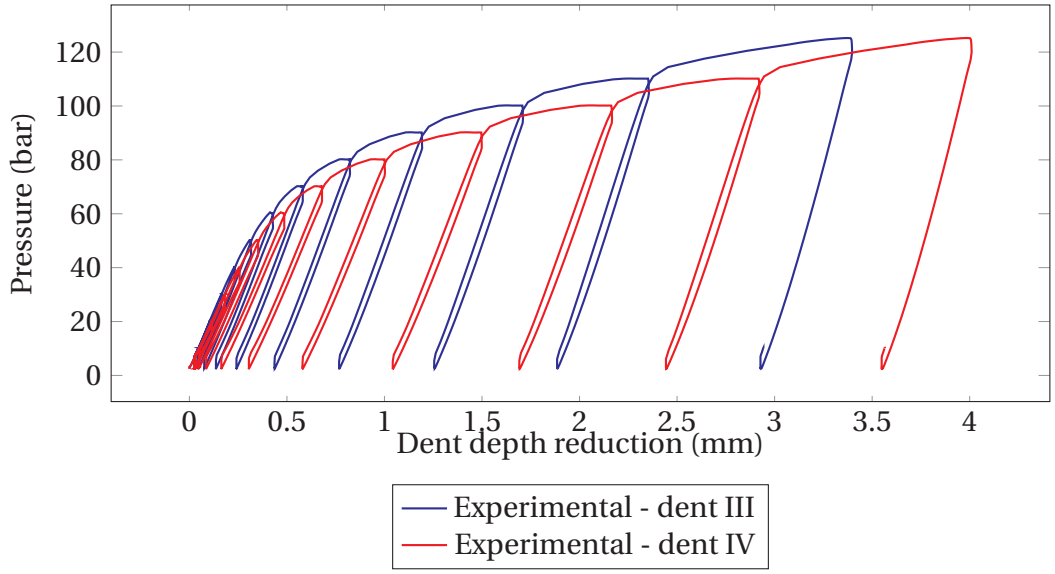

Figure D.2: Dent depth versus internal pressure for dent III - IV

Appendix E

Results from experimental testing

The following part shows all the strain results plotted with strains versus pressure.

E.1 Run 1

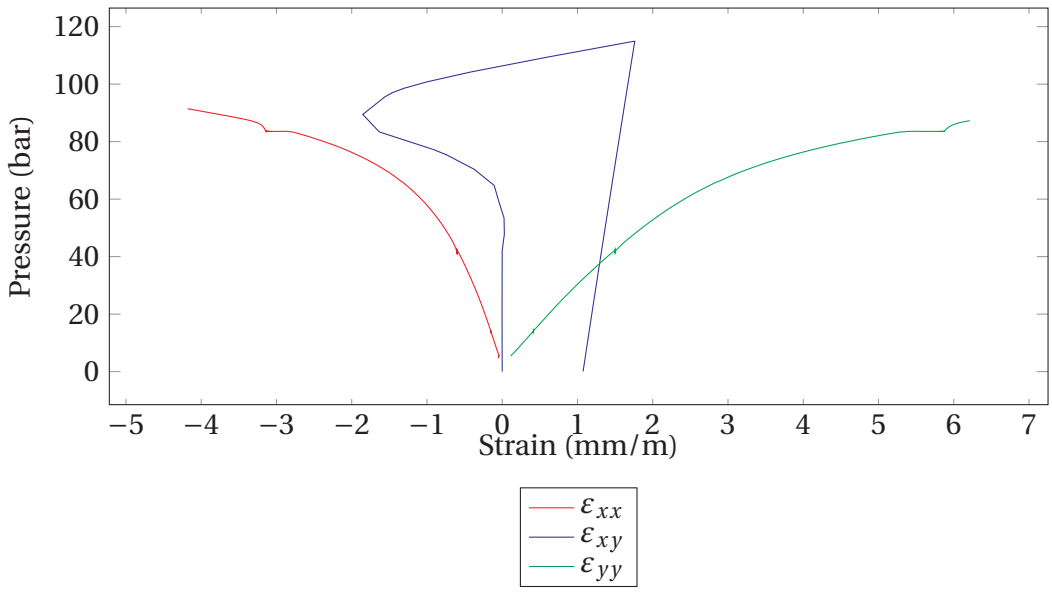

Figure E.1: Strains in dent I versus internal pressure - Gauge 1

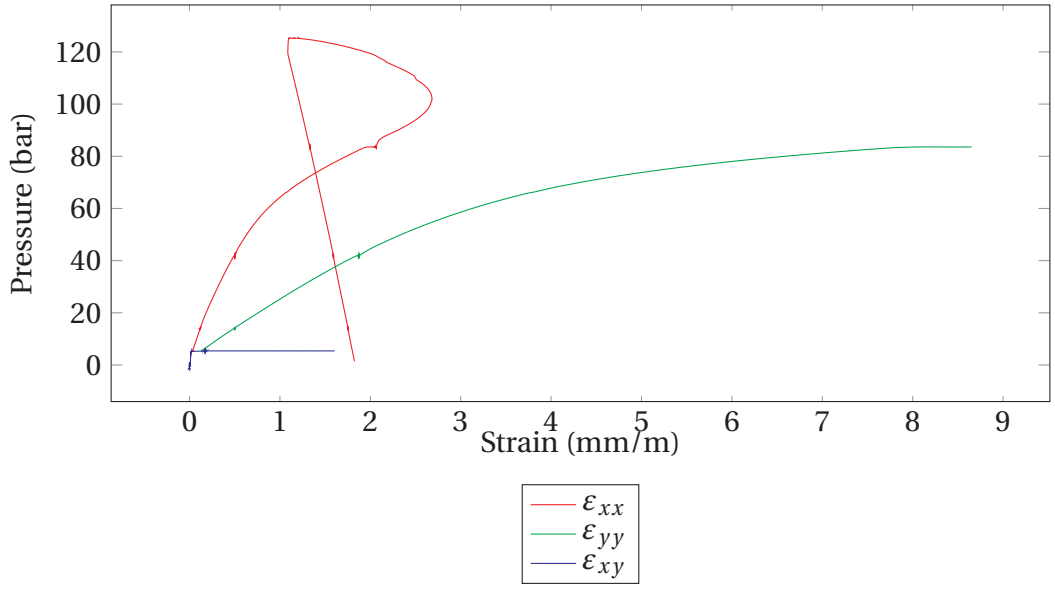

Figure E.2: Strains in dent I versus internal pressure - Gauge 2

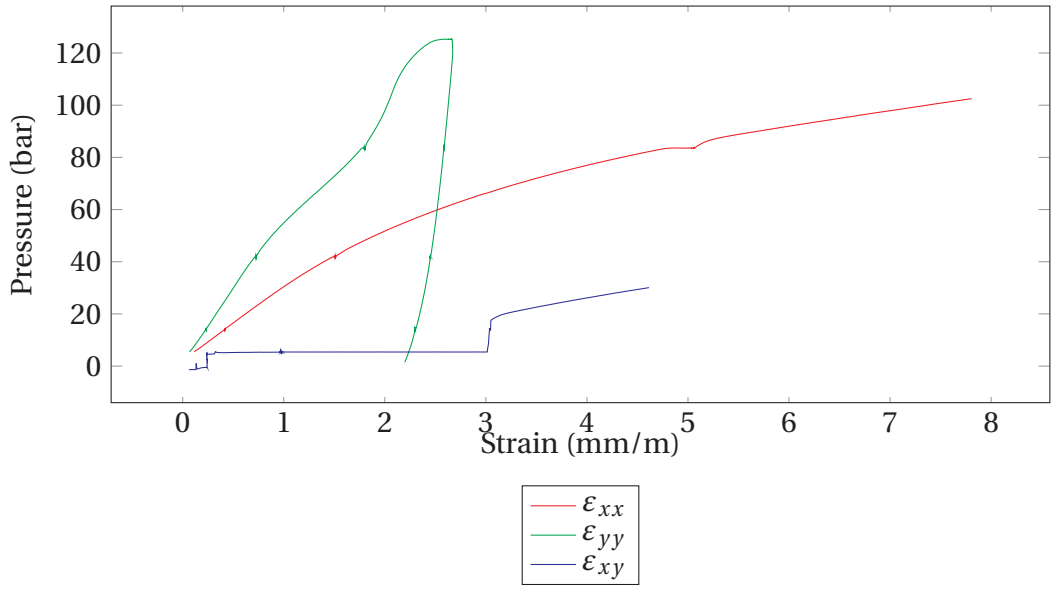

Figure E.3: Strains in dent I versus internal pressure - Gauge 3

E.2 Run 2

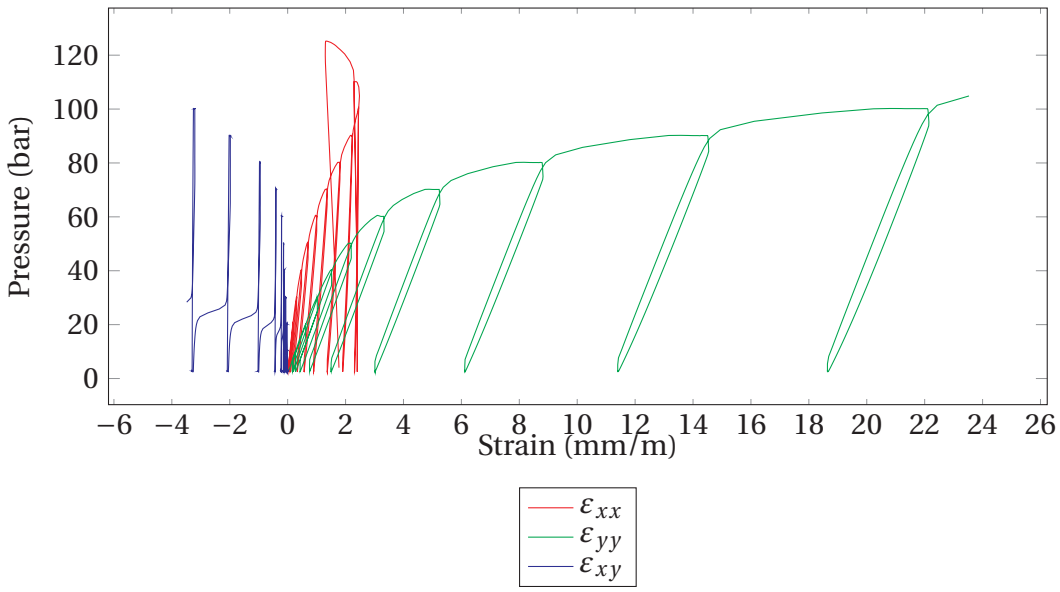

Figure E.4: Strains in dent II versus internal pressure - Gauge 1

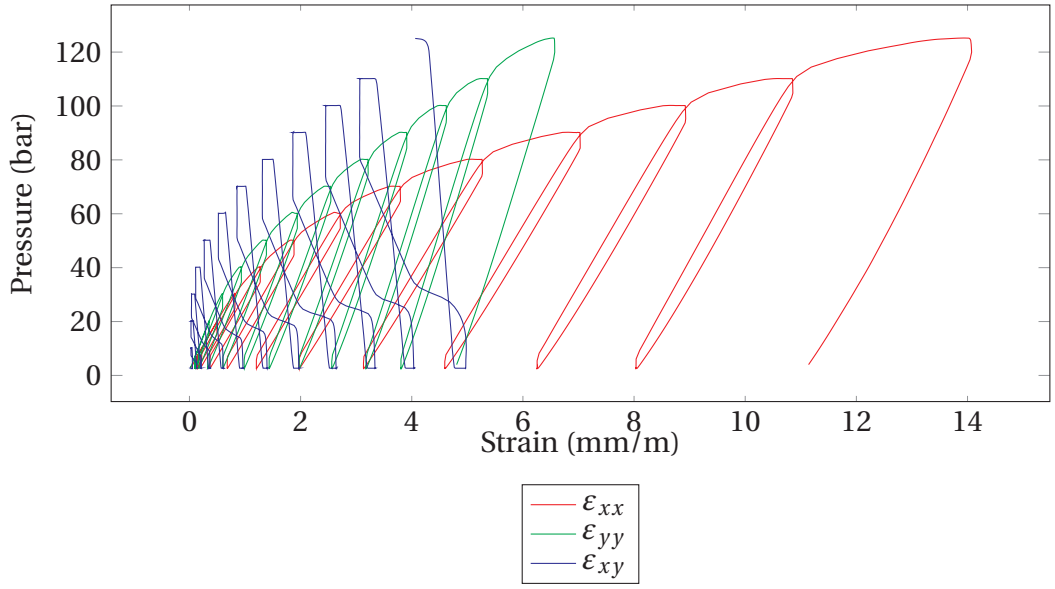

Figure E.5: Strains in dent II versus internal pressure - Gauge 2

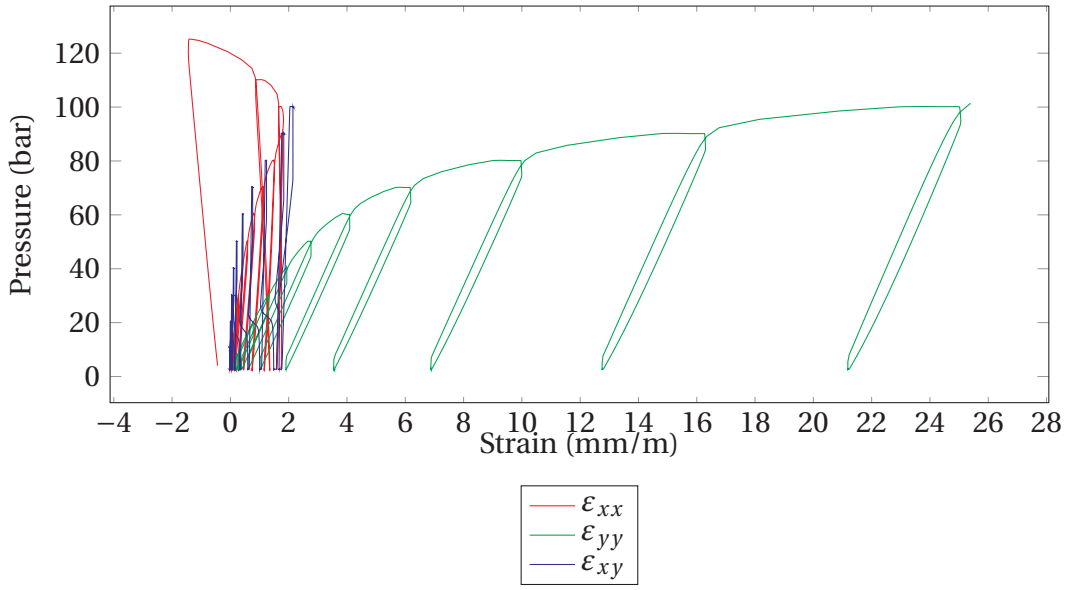

Figure E.6: Strains in dent III versus internal pressure - Gauge 1

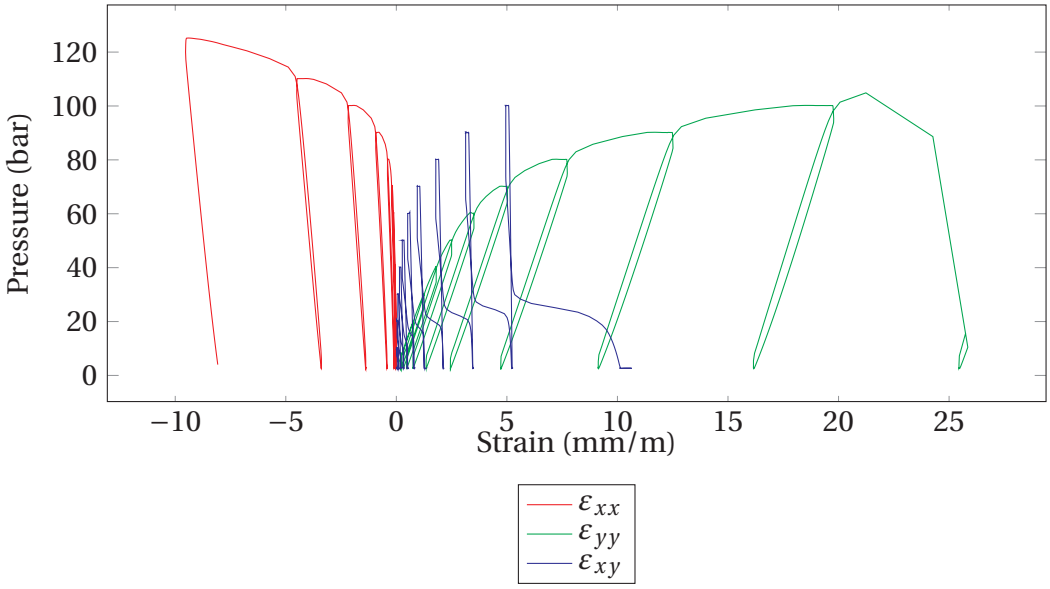

Figure E.7: Strains in dent III versus internal pressure - Gauge 2

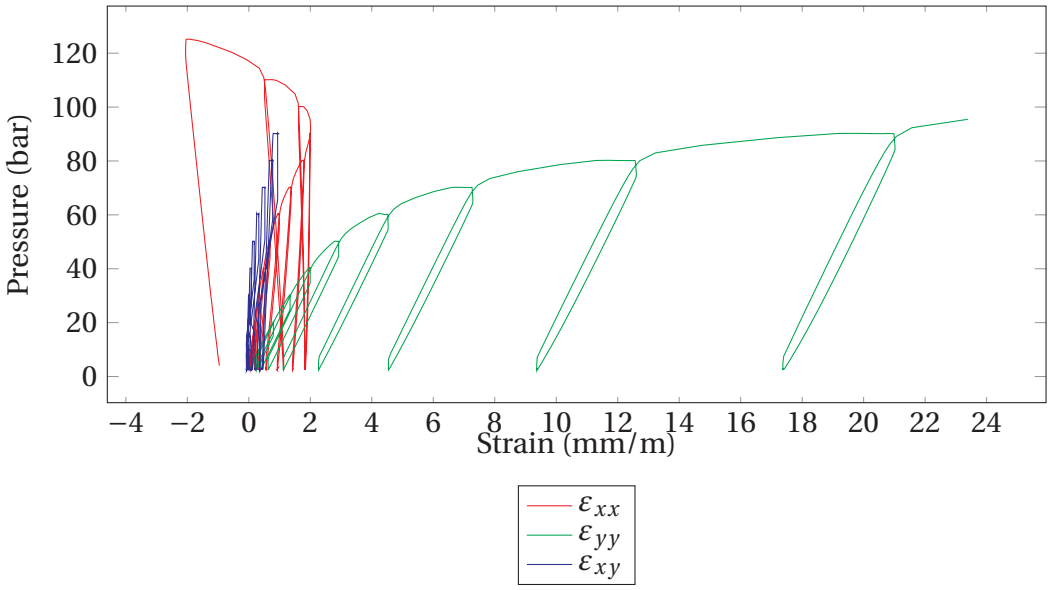

Figure E.8: Strains in dent IV versus internal pressure - Gauge 1

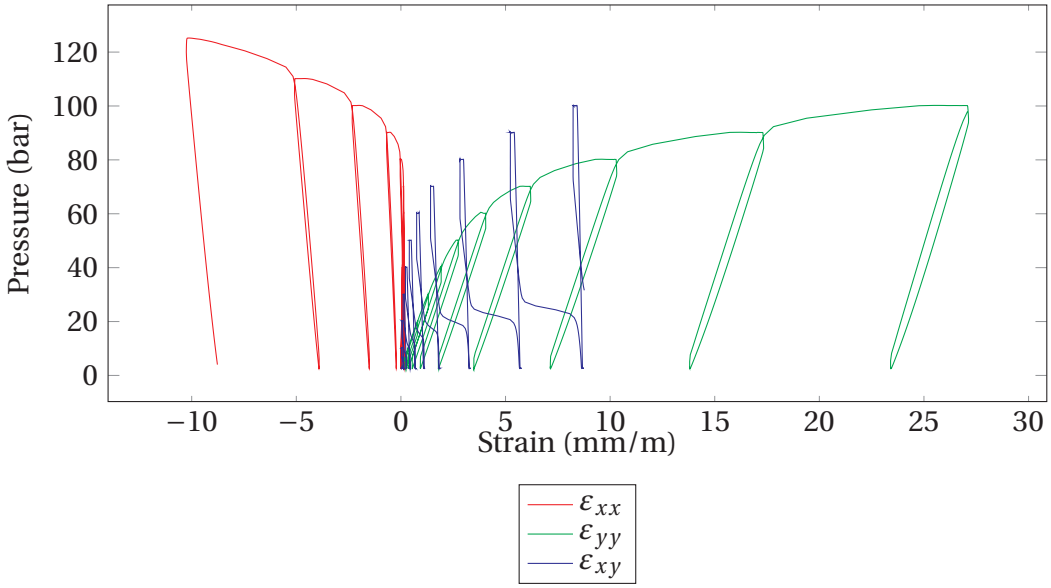

Figure E.9: Strains in dent IV versus internal pressure - Gauge 2

E.3 Run 3

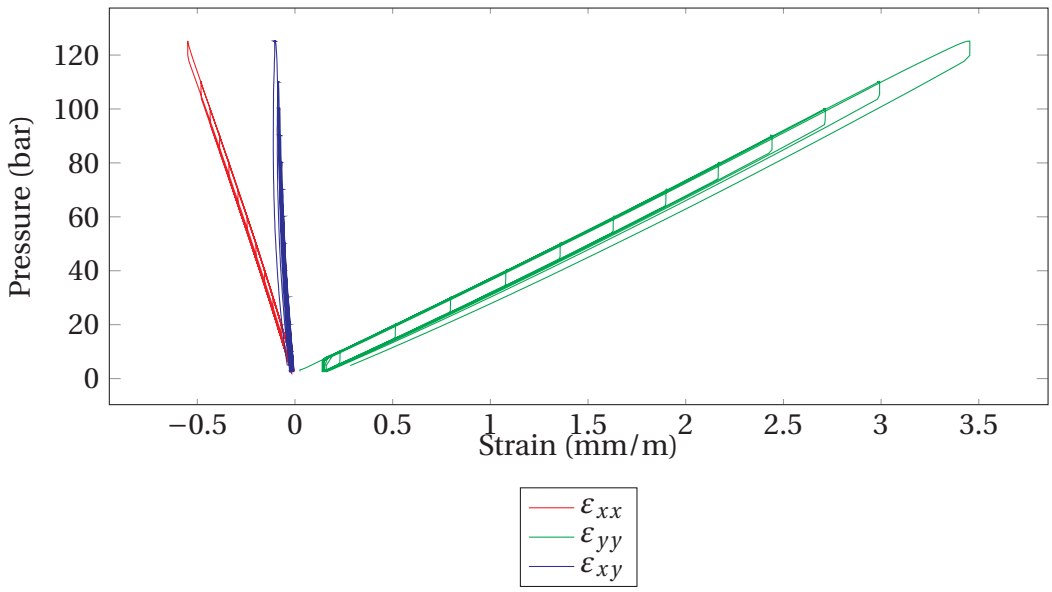

Figure E.10: Strains in dent II versus internal pressure - Gauge 1

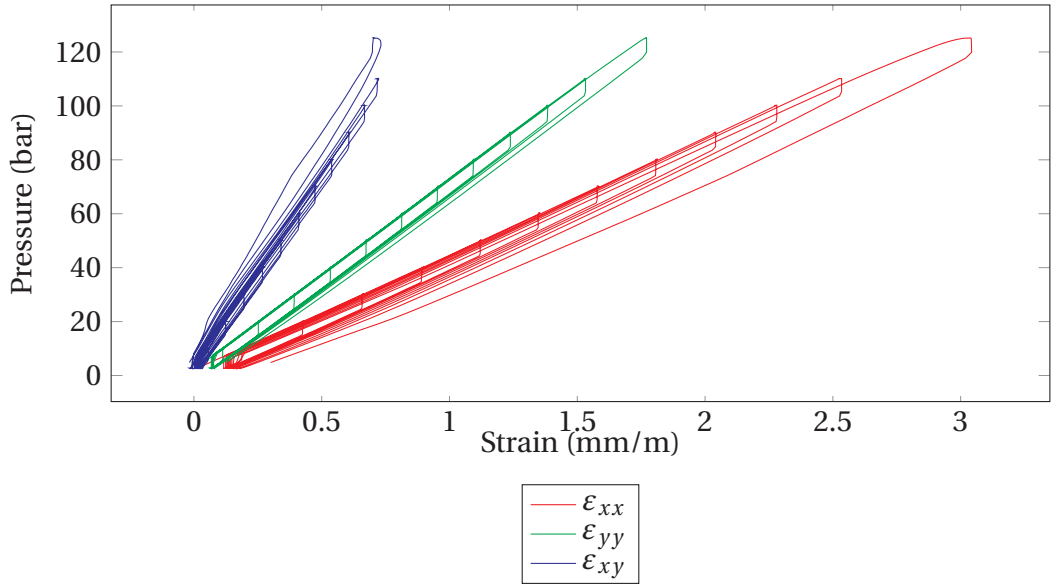

Figure E.11: Strains in dent II versus internal pressure - Gauge 2

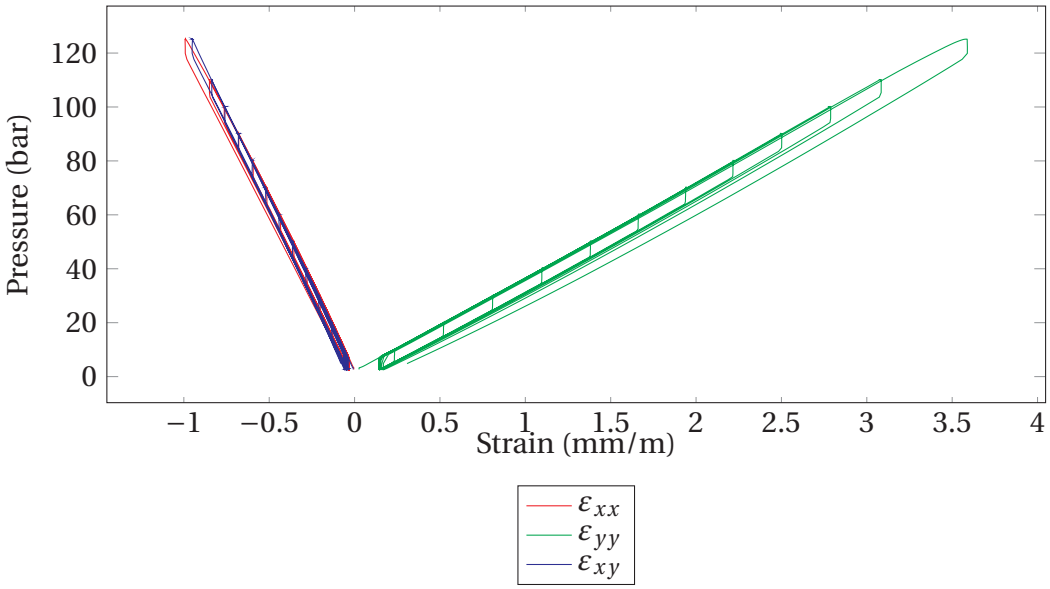

Figure E.12: Strains in dent III versus internal pressure - Gauge 1

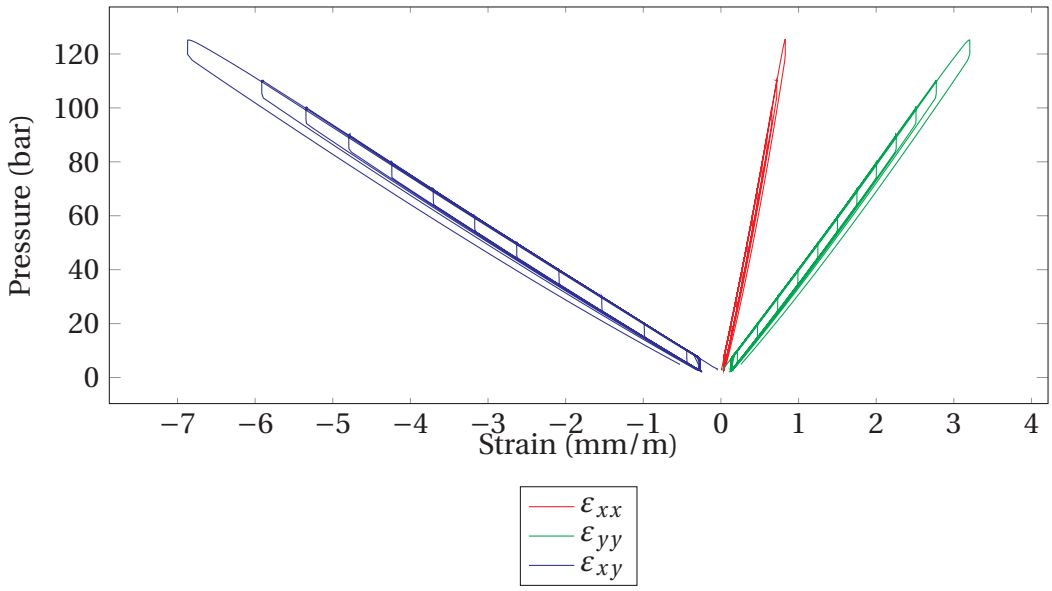

Figure E.13: Strains in dent III versus internal pressure - Gauge 2

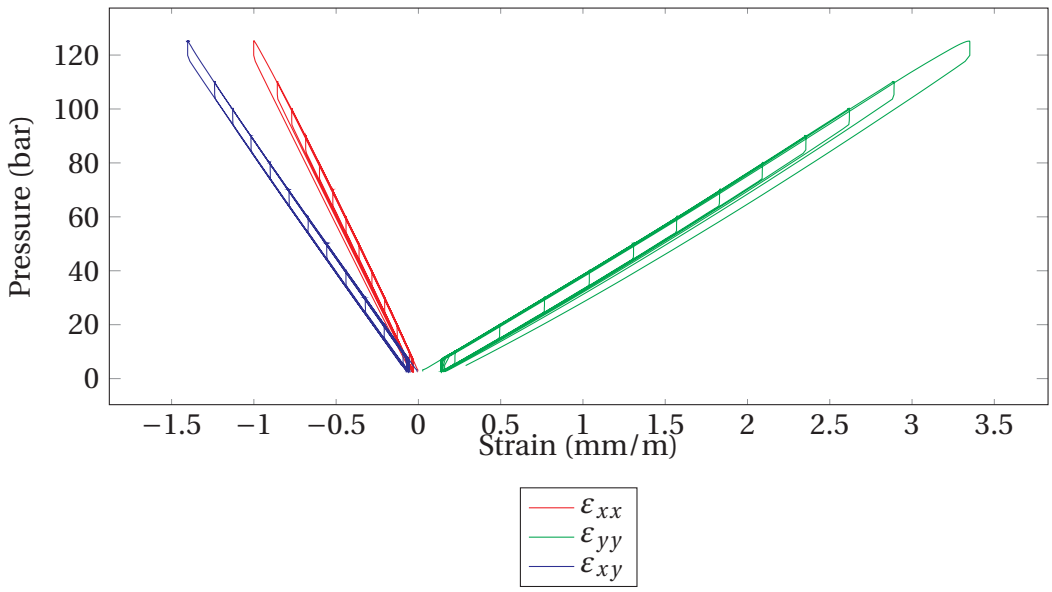

Figure E.14: Strains in dent IV versus internal pressure - Gauge 1

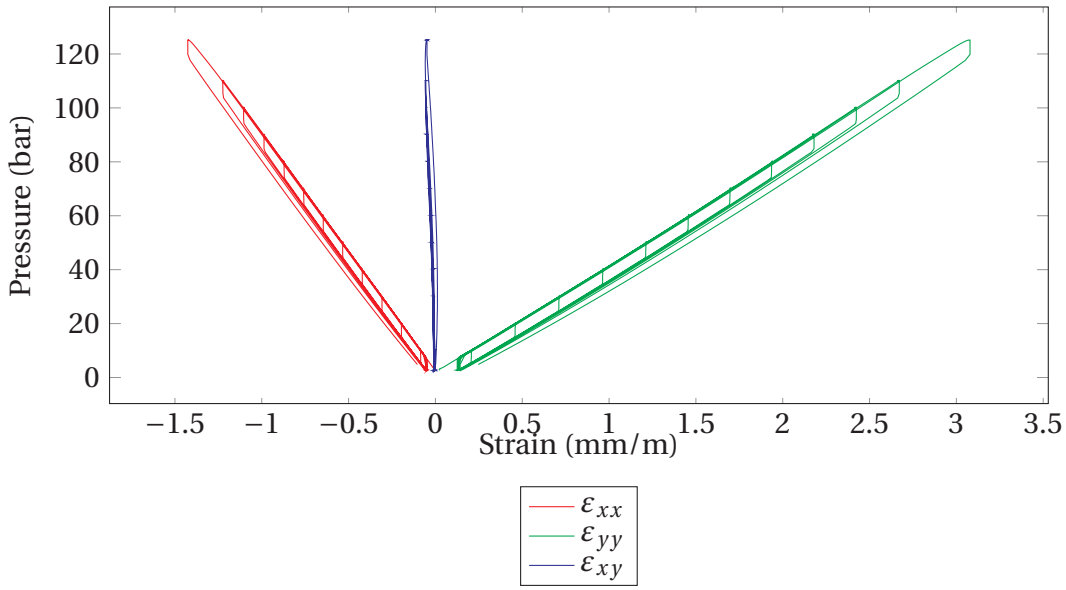

Figure E.15: Strains in dent IV versus internal pressure - Gauge 2